8-2013

A Compact, Convective Flow NaK Test Loop for Material Exposure Contained in an Argon Atmosphere

David Joseph Rowekamp
drowekam@utk.edu

To the Graduate Council:

I am submitting herewith a thesis written by David Joseph Rowekamp entitled "A Compact, Convective Flow NaK Test Loop for Material Exposure Contained in an Argon Atmosphere." I have examined the final electronic copy of this thesis for form and content and recommend that it be accepted in partial fulfillment of the requirements for the degree of Master of Science, with a major in Nuclear Engineering.

Martin L. Grossbeck, Major Professor

We have read this thesis and recommend its acceptance:

Arthur E. Ruggles, Lawrence H. Heilbronn

Accepted for the Council:
Dixie L. Thompson

Vice Provost and Dean of the Graduate School

(Original signatures are on file with official student records.)

A Compact, Convective Flow NaK Test Loop for Material Exposure Contained in an Argon Atmosphere

A Thesis Presented for the
Master of Science
Degree
The University of Tennessee, Knoxville

David Joseph Rowekamp
August 2013

Abstract

The objective of this research project was to construct a compact NaK loop to test weld configurations for application in a space reactor. The focus of this project is the construction of a compact test loop focusing on safety considerations for operating in university environment. The NaK loop fits inside of standard welding glove-box, and holds 64 weld specimens and a diffusion bonded tube-plate assembly. The NaK loop has a furnace which operates at a 650 degrees Celsius. It contains two independent and by-passable cold traps to maintain low oxygen levels in the NaK. The loop also contains a coil heat exchanger to cool the NaK. The loop operates with purely with convective flow, which is driven by the temperature differential between the furnace and the heat exchanger. Convective flow was confirmed at the furnace temperature of 250 degrees Celsius by monitoring temperature behavior. At the operating temperature of 650 degrees Celsius, a flow velocity of 3 millimeters per second was measured. The flow velocity was measured by tracing an induced heat spike as it moved in the system.

Table of Contents

List of Tables

List of Figures

Chapter 1

Introduction

For over 50 years, liquid metals have been investigated as alternative coolants for producing nuclear power. The interest in liquid metals comes from specific advantages they have over water as a coolant for power generation and in some aspects of safety. In terms of power generation, the most prominent of these advantages is the increased power density available with liquid metal as opposed to light and heavy water. This increase in power density stems largely from the greater thermal conductivity of liquid metals compared to the traditional water coolants. In terms of safety, liquid metals typically have boiling temperatures above the maximum operating temperature for a reactor, resulting in no gaseous phase change which greatly reduces operating pressure. This reduction in operating pressure helps to reduce the severity of a loss of coolant accident due to a system rupture. In addition to their high boiling temperatures, liquid metals also have a high heat capacity which increases thermal inertia thereby reducing the chances of accidental overheating. Several liquid metals that have been studied for coolant use can be seen in Table 1, alongside their boiling and melting points.

Table 1: Liquid Metal Coolants

Coolant	Melting Point	Boiling Point
Mercury	-38.83°C	356.73°C
Sodium	97.72°C	883°C
NaK	-12.6°C	785°C
Lead	327.46°C	1749°C
Lead-bismuth	123.5°C	1670°C

Despite the general benefits of liquid-metal coolants, all liquid-metals increase the difficultly of repairing and maintaining the systems they are used in. These difficulties stem from the liquid metals being toxic, reacting strongly in the earth's atmosphere, or solidifying at room temperature. Each of the liquid metals listed in Table 1 has its own unique disadvantages regarding its use. Mercury, despite being the first coolant used in a liquid metal reactor (Clementine reactor), suffers from several disadvantages: low boiling point, toxicity, noxious fumes, high neutron cross-section, and a low thermal conductivity compared to other liquid metals. Sodium also has several disadvantages: it can ignite on contact with air, it reacts violently with water, it is not liquid at room temperature, and it can neutron-activate creating a radioactive liquid. Lead has a high melting point making it difficult to service and refuel a reactor due to the liquid solidifying. NaK and lead-bismuth are eutectic alloys, which give them a lower melting point than their pure components. This allows NaK to be liquid at room temperature, while increasing its air and water reactivity due to potassium's increased chemical

reactivity compared to sodium. Lead-Bismuth has a much lower melting point than pure Lead, but it is also highly corrosive to most structural metals, in particular martenistic and austenitic stainless steels [1]. Do to this mixture of advantages and disadvantages, liquid metals have typically been used only when their advantages are required and in fast breeder reactors where water is not a viable option.

Interest in liquid metal research for nuclear reactors greatly diminished during the 1970s as increased cost for breeder reactors made them non-economic [2]. This decline has led to a decrease in the ability to support and general knowledge of small scale liquid metal testing, particularly locations to analyze the interstitial oxygen content in sodium. However, in recent years lead has become a design consideration for generation IV power reactors due to safety options and modular reactor cores that could be swapped out, mitigating the need to clean a core with solidified coolant. Also, NaK has become an advantageous option for space operations due the lack of water and atmosphere, the low operating pressure, weight reduction, and the removal of the need for a coolant melt. Thus, part of this research project is an attempt to adapt older methods to modern requirements, and to reinvestigate and improve simplified laboratory methods that may have been lost over the years or ignored over the years.

NASA has recently begun developing Fission Power Systems (FPS) for space applications. A primary goal is developing technology options for long term missions at lunar outposts and future missions to Mars. The initial designs are meant to operate for eight years without maintenance or refueling. The conceptual reactors utilize NaK in both the primary and intermediate loops as liquid metal coolant. The primary loop will

operate at temperatures exceeding 600°C, and heat exchangers and piping will be comprised of AISI Type 316L stainless steel. One of the life expectancy concerns stems from the interaction between the welds and the high temperature coolant in the intermediate heat exchangers. The intermediate heat exchangers have several dozen tube-plate welds that could be a concern for several years of operation. Since life expectancy and weld configurations have not been studied for 316L stainless steel welds in NaK, endurance testing needs to be performed on viable weld options at expected operating conditions. Thus, the primary purpose of this research project is to construct a NaK test loop for testing welds at the conditions expected in the intermediate heat exchanger.

1.1 Problem Statement

Due to the reduction of liquid metal testing in recent decades a lot of information and knowledge pertaining to previous test loops has been buried or lost as common knowledge has been forgotten. The goal of this project is to fabricate a NaK loop in a safe, inert environment to be used to test weld methods for space reactor fabrication. The project focuses on the real time exposure of tube-plate weld specimens in order to project the expected failure of a heat exchanger based on the conditions of weld configuration, and material thickness.

This research will produce a streamlined NaK system that is small enough to fit in a moderately sized welding glove box (approx. 70 cm X 70 cm X 120 cm). The system will include a furnace chamber, a method to generate NaK flow, measurement of NaK flow, and a purification method for the NaK.

1.2 Contributions of the Thesis

This thesis provides an overview of the options that exist for constructing a liquid metal loop, highlighting their advantages and disadvantages. In addition, the actual construction and use of a liquid metal loop allows for the information and techniques to be applied to larger and more involved test structures.

This thesis includes an analysis of the different methods of generating NaK flow that also reduce the risk of atmospheric exposure. The majority of methods presented are based on the use of magnetic fields and electricity to generate movement in a conducting fluid. However, the method of flow generation used in the system constructed is actually convective flow created by a temperature differential.

The thesis also highlights the different methods of flow measurement that are safe to use with NaK as the flowing liquid. The concerns about each method are also portrayed, allowing an informed decision to be made. The method used in the loop made is actually an indirect method, which requires a small heat spike to be generated in the loop and then traced around the system to measure the flow rate.

Chapter 2

Literature Review

Electrical power generation has been a primary concern of space missions since their inception. Nuclear power systems have been one of the standard options to provide sufficient, long-term electricity generation. The systems that have been utilized can be broken into two distinct groups, fission reactors and radioisotope power generators. Radioisotope power generators can be further broken into radioisotope thermoelectric generators and Stirling radioisotope generators (RTGs and SRGs). RTGs use the passive decay heat from radioisotopes (typically Pu-238) to generate electricity with static thermoelectric elements. SRGs use the passive decay heat from a radioisotope (Pu-238) in order to heat Helium and move a piston to generate electricity. Space fission reactors have been investigated to fill two distinct roles: nuclear propulsion, where fission energy is used to heat gas which is then expelled for thrust, and nuclear energy, where fission energy is used to generate electricity.

These radioisotope power generators are excellent at providing long-term kWh/day levels of electricity. However, some missions may require years of MWh/day levels of electricity such as a moon base or large scale laboratory. Currently, the best option to fulfill such electrical needs is a compact, fission reactor. As previously discussed, liquid metal reactors, in particular NaK-cooled reactors, provide a high power density making them an ideal option for a high-powered electrical source that takes up less mass. However, maintenance on a space reactor would be difficult, costly, and potentially dangerous. As such, there is a need for information on how long a NaK

reactor could potentially run before a major failure occurs or maintenance would be required. The approach to determine the life-span of a NaK space reactor was done by evaluating the common structural failure sites and failure modes of terrestrial NaK reactors. The most likely failure location and mode was determined to be the welds in the heat exchanger [16]. However, there are several weld standard configurations available for the proposed tube-plate welds in the heater exchanger. As such, a matrix of candidate weld configurations was needed to identify if any specific configurations would be advantageous. The specimen matrix can be seen in table 2. An additional weld option is also being investigated, which utilizes two welds: a sealant weld between the lip of the plate and the tube, and a diffusion bonded weld between a plate and the tubes. The assembly of the diffusion bonded weld option can be seen in figure 1, from which samples will be cut after exposure. With the candidate weld specimens identified, a method of testing the life expectancy of welds in a NaK space reactor was needed.

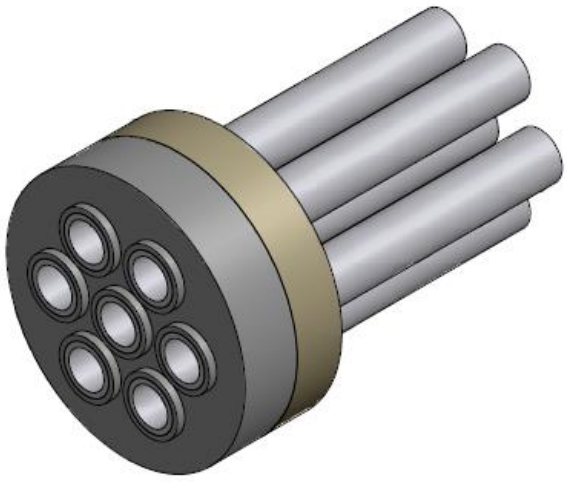

Figure 1: The diffusion bonded weld assembly.

Table 2: Specimen Test Matrix for the Project

		TIG (ORNL)			**Electron Beam**	**TIG (Novatech)**		**Thicker Pipe**
Time		3 months	1 year	3 year	1 year	3 months	1 year	1 year
Flush Weld	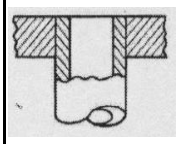	F-J-0-1	F-J-1-1	F-J-3-1	F-E-1-1	F-W-0-1	F-W-1-1	F-T-1-1
		F-J-0-2	F-J-1-2	F-J-3-2	F-E-1-2	F-W-0-2	F-W-1-2	F-T-1-2
Extended Weld	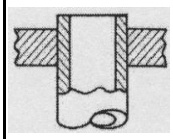	E-J-0-1	E-J-1-1	E-J-3-1	E-E-1-1	E-W-0-1	E-W-1-1	E-T-1-1
		E-J-0-2	E-J-1-2	E-J-3-2	E-E-1-2	E-W-0-2	E-W-1-2	E-T-1-2
Recess Weld	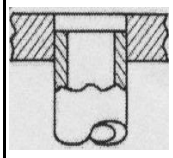	R-J-0-1	R-J-1-1	R-J-3-1	R-E-1-1	R-W-0-1	R-W-1-1	R-T-1-1
		R-J-0-2	R-J-1-2	R-J-3-2	R-E-1-2	R-W-0-2	R-W-1-2	R-T-1-2
Groove Weld	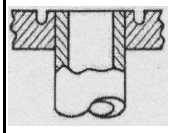	G-J-0-1	G-J-1-1	G-J-3-1	G-E-1-1	G-W-0-1	G-W-1-1	G-T-1-1
		G-J-0-2	G-J-1-2	G-J-3-2	G-E-1-2	G-W-0-2	G-W-1-2	G-T-1-2

	TIG (ORNL)		**Electron Beam**	
	3 months	1 year	3 months	1 year
Butt Welds	B-J-0-1	B-J-1-1	B-E-0-1	B-E-1-1
	B-J-0-2	B-J-1-2	B-E-0-2	B-E-1-2

The method of testing the welds involved exposing samples to NaK at conditions comparable to those expected in an actual reactor. Thus, a test loop needed to be developed to test the samples. Most important was that the testing conditions provided similar modes of degradation for the test welds. The primary modes of degradation for welds in a NaK reactor are expected to be thermal stress, grain boundary penetration, and ion transport. Ion transport is diffusion of ions out of structural materials in a hot section of loop and the depositing of the ions in the cold section of a loop. The two requirements for this to occur are a significant temperature differential and flow of the NaK. Thus, a test system needs a way of locally heating the NaK to 650°C (a furnace), a method to cause NaK flow, a method to confirm or measure NaK flow, and a method to maintain NaK purity conditions similar to those in a NaK space reactor.

2.1 NaK Circulation

Several approaches exist for generating NaK flow in a system or test loop. The most common approach is a pump system. However, this is a very diverse and varied approach for NaK and other liquid metals. The first approach is an electromagnetic pump (EM pump). The options and methods for creating an EM pump are varied, but all methods use applied magnetic fields and conducted or induced electrical currents on a conducting fluid (NaK) to generate a net perpendicular force on the fluid. A second approach is the use of a mechanical pump, which is similar to a common pump for water. Finally, the third approach is the use of convective flow to generate fluid (NaK) flow.

2.1.1 Conduction Electromagnetic (EM) Pumps

Conduction EM pumps operate by applying an electric current and a magnetic field perpendicularly to each other in a conducting fluid in order to move the conducting fluid in the third perpendicular direction. An example showing a simple conduction DC EM pump and the appropriate orientation of the current and magnetic field can be seen in Figure 2. Conduction EM pumps can be grouped into two general categories: ones that use DC current, and ones that use AC current. Both groups still apply a current through the conducting fluid, but the AC variation makes use of two sets of electromagnets and current electrodes. Both options provide unique benefits and disadvantages with their use.

A conduction DC EM pump has the simplest geometry and is relatively easy for an individual to manufacture. They are also the easiest to understand and quantify with a mathematical model. The magnitude of the force applied to the liquid can be determined

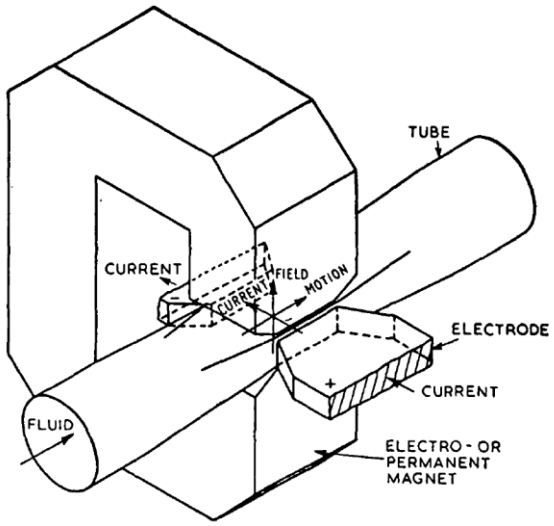

Figure 2: Simple DC Electromagnetic Pump [3].

using: $F = BI_e r / 10 \ dynes$, where **B** is the magnetic flux density in the liquid in gauss, $\mathbf{I_e}$ is the current in amperes that traverses through the magnetic field, and **r** is the width of the pipe in centimeters parallel to the direction of the current [4]. The developed pressure can be found using: $P = BI_e r /(10rs) \ dynes / cm^2$, where **s** is the width in the magnetic field direction in centimeters [4]. Flow rate, Q, in cubic centimeters per second can be approximated using: $Q = \frac{10^8 s}{B}\left[I\left(\frac{R_w R_b}{R_w + R_b} \right) - \frac{10Ps}{B} * \left(R_e + \frac{R_w R_b}{R_w + R_b} \right) \right] cm^3 / \sec$, where I is the total current in amperes, R_w is the resistance of the tube wall bypass, R_b is the resistance of the liquid metal bypass (current through the liquid, outside the magnetic field), and R_e is the resistance of the liquid metal in the magnetic field [4]. Estimating the resistances of the three pathways can be a challenge without extra experiments or available experimental references, in particular the liquid bypass resistance. The main

drawback to this EM pump is that it requires a high current (~20 amperes) at a low voltage (~1V) in order to function at a reasonable level, which requires the fairly difficult development of a power-processing unit [5]. In addition, the low efficiency of a DC EM pump can turn it into a power drain concern depending on the application [6].

Another option is to use an AC conduction EM pump. Such a pump is another step more completed than its simpler DC brother. One of the simpler versions requires two current transformers and four windings on the magnetic yokes, as seen in figure 3. However, the basic behavior of the pump can be generalized as two DC conduction pumps in series with directions of both the current and magnetic field on one pump opposite to the current and magnetic field directions on the other pump. Like the DC pump, the simplified rectangular geometry allows for straight forward calculations, although phase and frequency are now additional variables. Also, the use of an AC pump

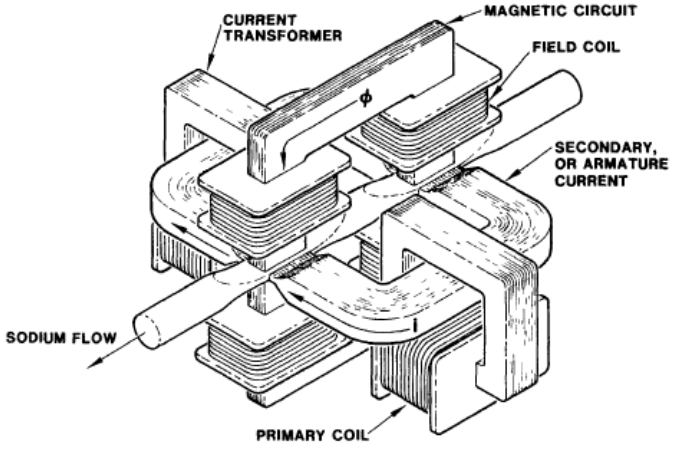

Figure 3: An AC conduction EM pump [7].

results in a time varying force due the varying nature of the applied magnetic fields and the applied currents [5]. This varying force can result in vibrations and noise throughout the system, which is an important concern for long term functionality [5].

Although the mathematics of an AC conduction EM pump is slightly more complicated, it is well understood and easily calculated on a theoretical level. The current and magnetic field being applied in an AC conduction pump can be described using: $I(t) = I_{\max} \sin(\omega t \pm \theta)$, $B(t) = B_{\max} \sin(\omega t)$, where ω is the frequency and θ is the phase difference between the current and magnetic field [5]. The force applied to the liquid can be calculated using: $F(t) = B_{\max} I_{\max} \left[\frac{(1 - \cos(2\omega t))\cos(\theta) \mp \sin(2\omega t)\sin\theta}{2} \right] w$, where w is the width of the pipe in the direction of the current and the $\mp$ accounts for sign changes resulting from θ [5]. The fluid pressure increase from the pump can again be found by dividing the force applied by the cross-sectional area: $P(t) = \frac{F(t)}{sw}$, where s is the width of the pipe in the direction of the applied magnetic field [5].

The major advantages and disadvantages of using an AC conduction EM pump can be summarized in the following manner. The primary advantage of AC is its ability to generate a high current, low voltage power electrical source for the pump easily. On the other hand, the AC conduction EM pump complicates the pump design to a significant degree, adding several coils and transformers compared to the DC conduction EM pump. The addition of coils and transformers leads to a large increase in mass and volume.

2.1.2 Stationary Induction Electromagnetic (EM) Pumps

There many variations and options that exist for using an induction EM pump. As such, this section will focus on induction pumps with no moving parts, and will review the annular linear induction pump (ALIP), the coil induction pump (CIP), and the flat linear induction pump (FLIP). These are not the only induction pump designs available, but they appear to be the types used most.

All induction pumps operate on the same basic principle. In nearly all cases a time varying current passes through sets of wires wrapped around iron cores producing a magnetic field that travels through the conducting fluid as a wave with a given phase velocity [5]. The magnetic field induces a current in the fluid, which interacts with the traveling magnetic field, generating a net Lorentz force on the liquid metal or other conducting fluid [5]. This is illustrated in figure 4 for a FLIP and figures 7 and 8 for an ALIP.

The flat linear induction pump (FLIP) is one of the simpler induction pumps and requires no magnetic core in the liquid metal, assuming the rectangular thickness of the

pipe is sufficiently short in the direction of the generated magnetic field. A representative drawing of a short section of a FLIP can be seen in figure 4, which also highlights the directions of the current, the magnetic field, and the fluid flow. The FLIP suffers from losses due to its rectangular geometry, which does not fully contain the generated magnetic field leading to parts of the magnetic field applying no work on the liquid metal [5]. The result is that the FLIP is the least efficient of the induction EM pumps.

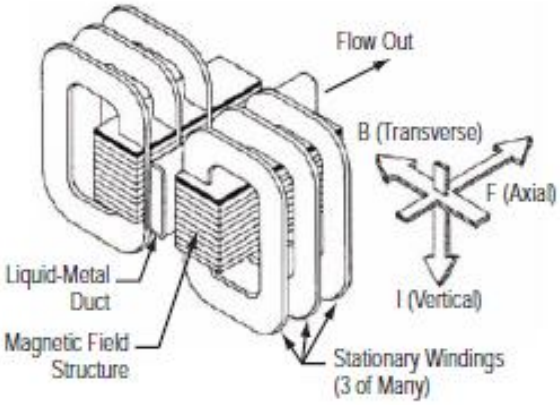

Figure 4: Drawing of a Flat Linear Induction Pump [5].

However, a FLIP is a more readily constructed induction pump. Thus, a basic FLIP was constructed and tested for its viability as an option for NaK flow in the test loop. The FLIP created used only one set of windings and an opposing ferromagnetic bar to complete the magnetic circuit, instead of a parallel set of windings. The FLIP was constructed using two iron bars and three copper coils wrapped around three steel cores as shown in figure 5. The pump was used on a tube filled with mercury and was powered

through a variac to control its electrical power supply. The test assembly can be seen in figure 6. The constructed FLIP created 11 mmHg of pressure at 10 amperes and 33 mmHg of pressure at 15 amperes. The copper wire used in the coils failed at 20 amps. This test showed that even a basic induction pump would have a positive effect on NaK flow. However, without cooling the coil, durability was a concern with the long term operation of the test loop. As such, induction pumps were considered a secondary option for generating NaK flow in this project's test loop.

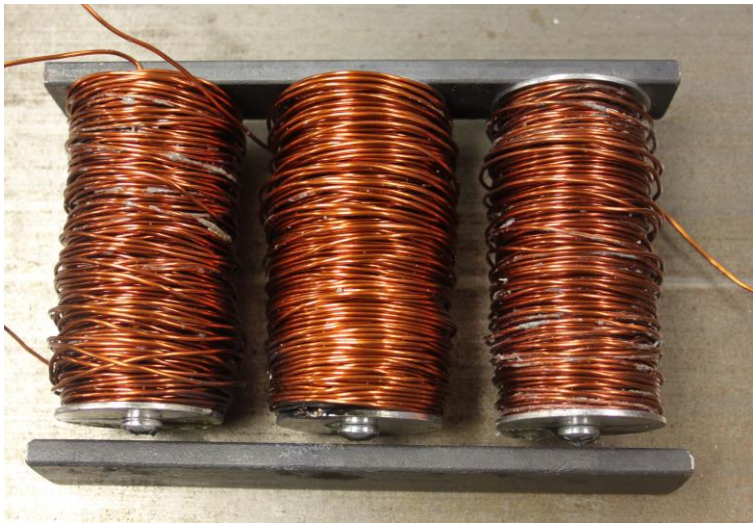

Figure 5: The constructed FLIP after testing.

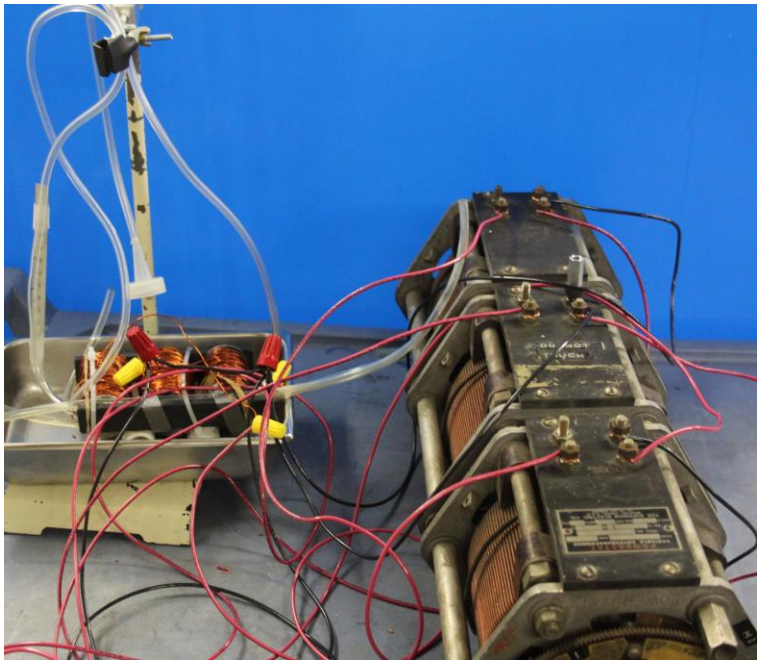

Figure 6: The FLIP test assembly is on the left which comprises of the FLIP pump in figure 5, a mercury filled tube, a steel pan, and a metric ruler. The variac is on the right was used to adjust current.

The annular linear induction pump (ALIP) operates on a concept very similar to the FLIP. The ALIP also uses time varying currents in its wires, but instead of creating a rectangular duct, a ferromagnetic core, or torpedo, is positioned in the middle of the pipe. The torpedo forces the liquid the metal to flow around and completes a magnetic circuit in order to generate the necessary field. A drawing of an ALIP can be seen in figure 7. Also, forcing the liquid metal to flow as a ring shortens the distance between the two magnetic poles, increasing the field strength and thereby increasing the force applied to the liquid metal. A sketch showing the generated magnetic fields and induced electric currents can be seen in figure 8.

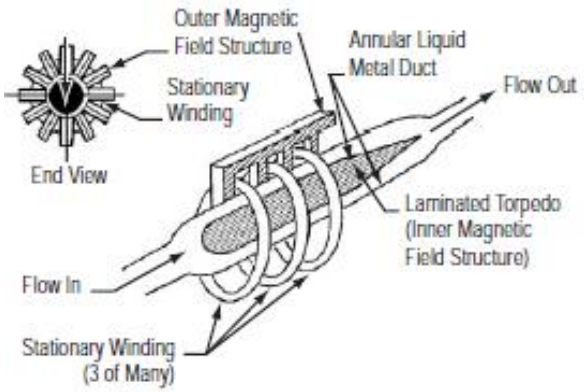

Figure 7: Drawing of an annular linear induction pump (ALIP) showing the basic geometry and orientation of its components [5].

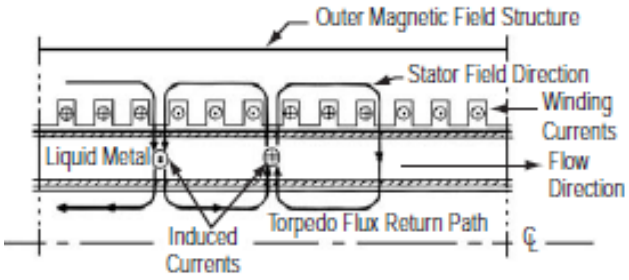

Figure 8: Representative drawing of the magnetic fields and induced currents in an annular linear induction pump (ALIP) [5].

The coil induction pump is a unique option, which generates its flow by applying a rotating twisted magnetic field. This type of pump utilizes a three-phase alternating current, which is passed through appropriate windings that are wrapped in a helical fashion around the pipe containing the liquid metal to be pumped. A rough example of this orientation is shown in figure 9. The magnetic fields rotate in the x-y plane and vary in the z direction, which can be seen in figure 10. This combination creates axial thrust in a similar fashion to the impellers of an axial-flow turbo pump, which generates its flow by rotating twisted metal in the x-y plane [8].

The induction pumps covered in this section represent only a small sample of the designs that have been developed. However, despite their differences, the variations of induction pumps share many general characteristics that allow for a reasonable comparison to other liquid metal pumping options. For the most part, induction pumps lose a great deal of efficiency and are troublesome to operate at low flow rates or power outputs [5]. Also, in smaller, low power systems the mass fraction of an induction pump tends to be quite large due to needing several groups of windings to produce the traveling magnetic wave [5]. Induction pumps also oscillate due to the phase velocity being faster than the flow rate of the liquid metal, making vibrations a potential system wide issue. Also, both conduction and induction EM pumps require sufficient heat removal, since high temperatures will degrade the stators in induction pumps. Finally, due to the complex interactions of eddy currents, Lorentz forces, and fluid flow development; induction systems are typically solved numerically due to the difficulties of an analytical solution.

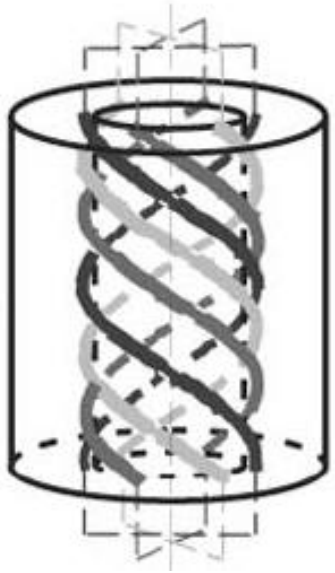

Figure 9: Example showing the windings of a tri-phase CIP [8].

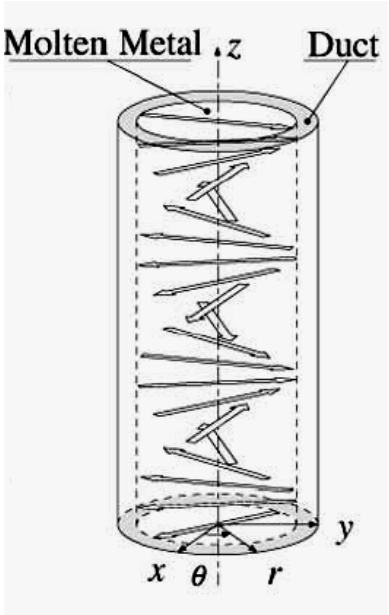

Figure 10: Diagram of the rotating twisted magnetic field in a CIP [8].

2.1.3 Rotating Permanent Magnet Induction Pump

In addition to the electrically driven induction EM pumps, there is a variation which operates by physically moving a magnetic field to create a traveling magnetic wave. In the methods discussed previously, electric phase changes or multiple phases were used to apply different and changing magnetic fields, which would allow a magnetic field to "travel" the length of the pump. This section introduces a method which moves permanent magnets with an electric motor to generate a magnetic field that is physically shifted. Figure 11 shows a simple example of a design configuration using this method. The magnets used in this design are oriented in an alternating "north"/ "south" sequence as shown in figure 12. The real advantages of this design stem from its simplicity to construct. There are no windings or complex electrical conditioning necessary, and the primary components consist of a ferromagnetic yoke, a strong permanent magnet on a rotating structure, and a motor to spin the structure. One of the more difficult aspects is using the thin, bent, and rectangular duct needed for the simpler rotating permanent magnet pumps, and integrating it into the rest of the system. Finally, several major efficiency losses occur in this system due to the running of a motor, the rectangular geometry, and always having some magnets not being in a position to apply work at any given time. Results from an optimized pump provided a pump efficiency of about 10% [9], which can be compared to conduction pumps having roughly 10% efficiency and an optimized ALIP having 46% [6]. Thus, the simplicity advantage of a rotating permanent

magnet is only slightly offset by its below average pump efficiency compared to other pumping methods.

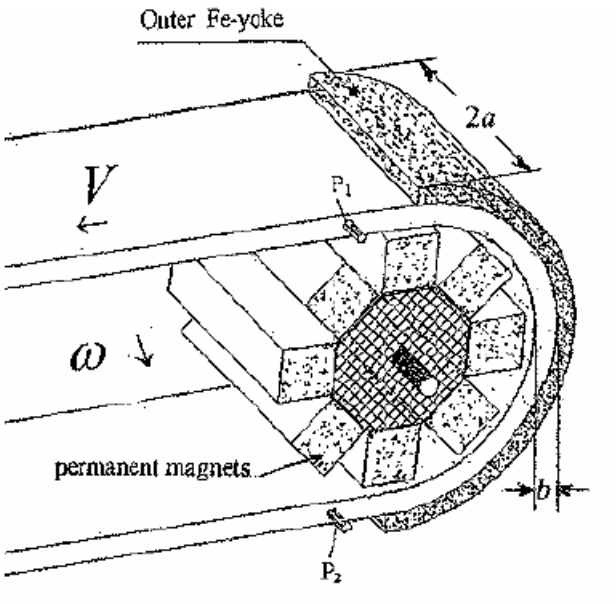

Figure 11: Example of simple rotating permanent magnet pump [9].

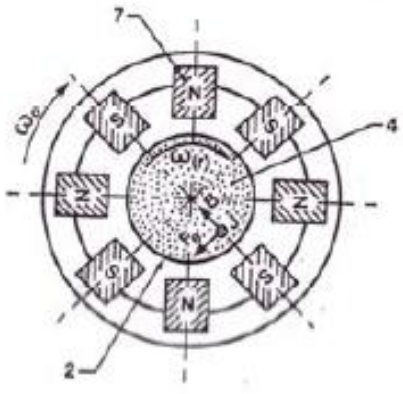

Figure 12: Diagram of the permanent magnets in a rotating permanent magnet pump [9].

2.2 NaK Flow Rate Measurements

Several options exist for measuring the flow of NaK or another liquid metal. One option is an electromagnetic flow meter which works in reverse of an EM conduction pump using a moving fluid and an applied magnet field to generate a current. Another option is a Venturi flow meter designed to withstand exposure to high temperature, flowing NaK. An additional option is to cause a heat spike in the NaK and track the spike's movement with attached thermocouples.

2.2.1 Electromagnetic (EM) Flow Meter

EM flow meters can be used on any electrical conducting fluid. They work in reverse of an EM conduction pump. In an EM flow meter, a magnetic field is applied perpendicularly to a moving, conducting fluid, which results in an electric current being generated perpendicularly to both the fluid flow direction and the applied magnetic field, as shown in figure 13. In practice either an electromagnet or a permanent magnet can be used, but typically a permanent magnet is more than sufficient, generating an emf that is at least a few millivolts [7]. The resulting flow rate due to field strength and emf generation rate can be calculated by solving the equations on the following page, and using figure 14 for the end effect correction factor and figure 15 for the magnet temperature correction factor [7].

$emf\ (mv) = \frac{QB(K_1)(K_2)(K_3)}{3162d(K_4)}$, where Q = flow rate (gpm); d = pipe inner diameter (in.); B = flux density (gauss); K_1 = pipe wall shunting factor; K_2 = end effect factor and can be found from figure 14; K_3 = magnet temperature factor and can be found from figure 15; K_4 = pipe expansion factor [7].

$K_1 = \frac{2d \times D}{D^2 + d^2 + ((p_1 / p_2)(D^2 - d^2))}$, where D = pipe outer diameter; p_1/p_2 = ratio of electrical resistivity (p_1 = NaK resistivity, p_2 = pipe wall resistivity) [7].

$K_4 = 1 + a(T - T_0)$, where a = coefficient of thermal expansion for the pipe, T = temperature (°F) [7].

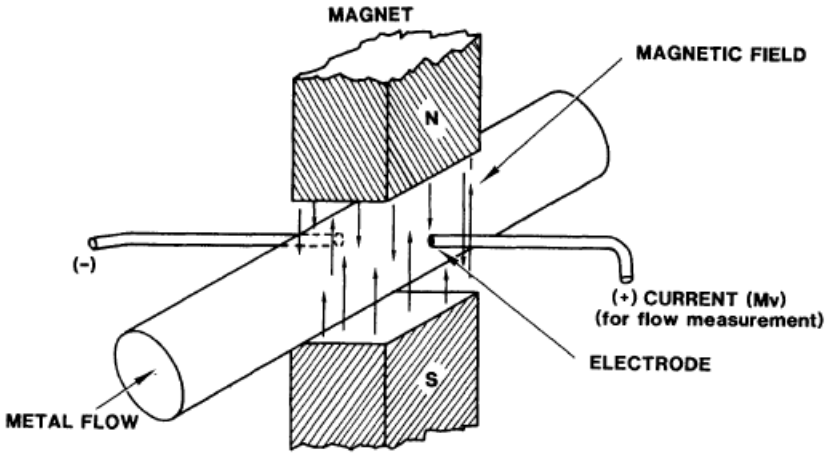

Figure 13: Concept drawing of an EM flow meter [7].

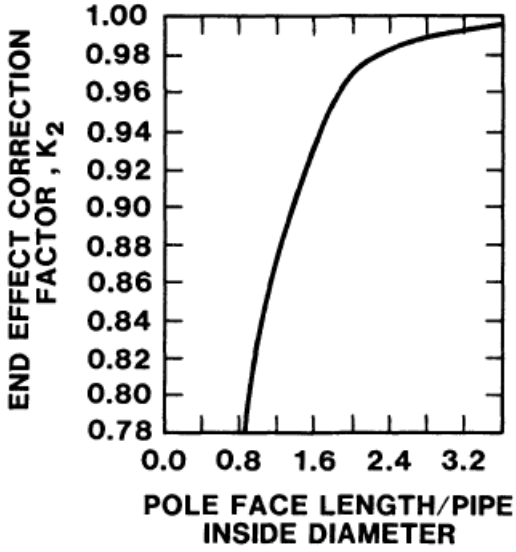

Figure 14: Chart for the end effect correction factor, K_2 [7].

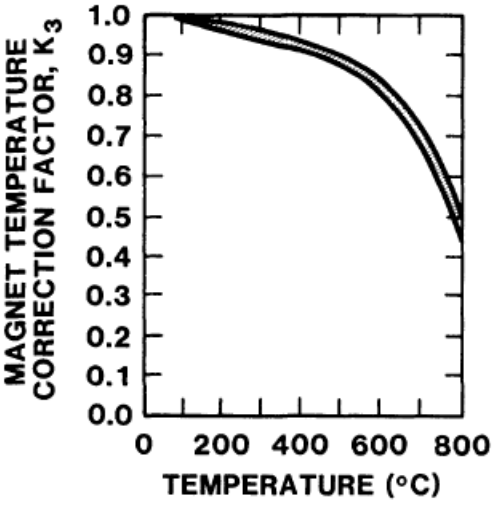

Figure 15: Chart for the magnet temperature correction factor, K_3 [7].

2.2.2 Venturi Flow Meter

The Venturi flow meter is a standard for measuring fluid flow in systems. The meter operates by utilizing the Bernoulli Effect, which involves reducing the cross-sectional flow area. This reduction causes a pressure difference between the original cross-section and the reduced cross-section. An example of a simple Venturi meter and the equation to calculate flow velocity can be seen in figure 16. It is important to note that the materials in the pressure gauges or in the manometer must be able to withstand potential interaction with the liquid metal and the conditions that may be applied. Venturi meters also result in a pressure drop that may adversely affect the flow rate in low flow systems.

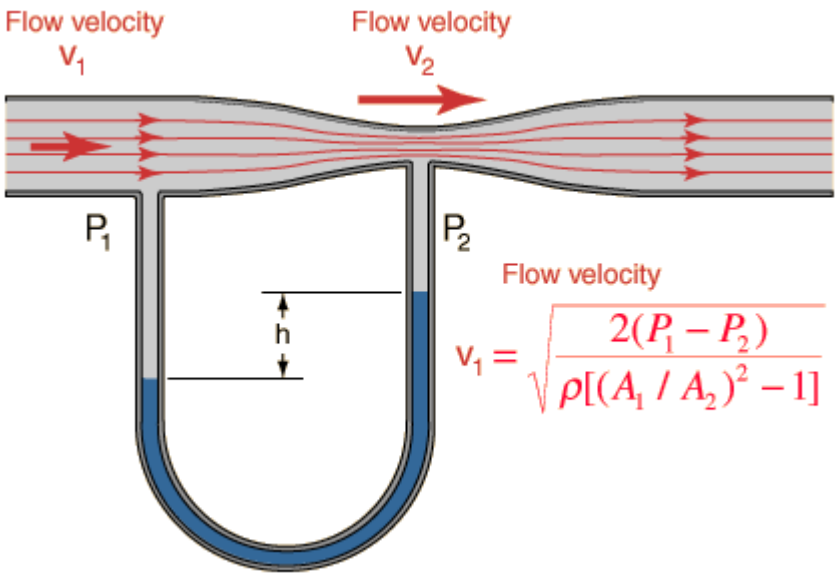

Figure 16: A basic Venturi flow meter design with the equation for calculating velocity from the two pressure measurements and the cross-sectional area at each pressure measurement location [12].

2.2.3 Heat Spike Tracing

A study done on a lithium loop is the primary reference for this approach [10]. The basic idea behind heat spike tracing is to first achieve a steady state operation of the system with constant temperatures. The next step is to apply a large, single heat burst to the system. After the heat spike is applied, the goal of the method is to track the temperature increases as the liquid metal flows around the system. By utilizing several thermocouples and a logging system it is possible to measure the fluid velocity by using the time and distance between the thermocouples.

In the lithium loop approach, a heated slug of lithium was created by heating part of the loop with a torch [10]. This slug was then tracked as it moved through the loop in order to determine the flow rate of the lithium. The system used in this project cannot use a torch due to the argon environment. Thus, a heating lamp was used in place of the torch. In addition, there is a concern as to identifying when the slug arrived at the measuring sites. Thus, the approach to identifying when the hot NaK slug arrived at a measuring site was investigated.

2.3 NaK Purification

2.3.1 Cold Trap

Cold traps appear to be the primary method that has been used to manage oxygen levels in sodium and NaK. Cold traps operate by lowering the temperature of the fluid in order to reduce oxygen's solubility in the liquid metal. A graph of oxygen's solubility in NaK can be seen in figure 17. The solubility of oxygen in NaK (78% K, 22%Na) behaves over the 90°C to 210°C range, as follows: $\log_{10}(S) = 7.09 - 2{,}795/T$, where S =

solubility (wppm), and T = absolute temperature (Kelvin) [13]. From this, it can be determined that NaK needs to be lowered to approximately 186°C in order to reduce solubility to 10 ppm. Thus, by lowering the temperature of NaK, oxides will form as oxygen precipitates out of the NaK. The oxides can then be caught and held with a monofilament stainless steel mesh or similar structure thereby removing the oxygen from the system. Cold traps vary greatly in their size and complexity depending on their operational requirements, and the determined limits on oxygen levels. In short, cold trap size increases as the volume of the liquid metal increases, and either cold trap complexity (i.e. multiple monofilament mesh passes) or size increases as purity demands increase. A diagram of a cold trap concept can be seen in figure 18. The basic cold trap unit used in this project is even simpler. The cold trap used is a 90° pipe bend filled with stainless steel wool and is placed after the cold leg of the system, instead of the cold trap requiring its own cooling system.

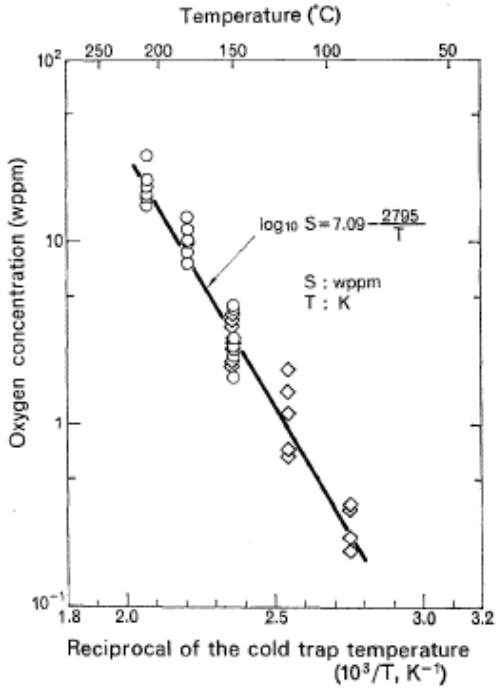

Figure 17: Solubility curve of oxygen in NaK [13].

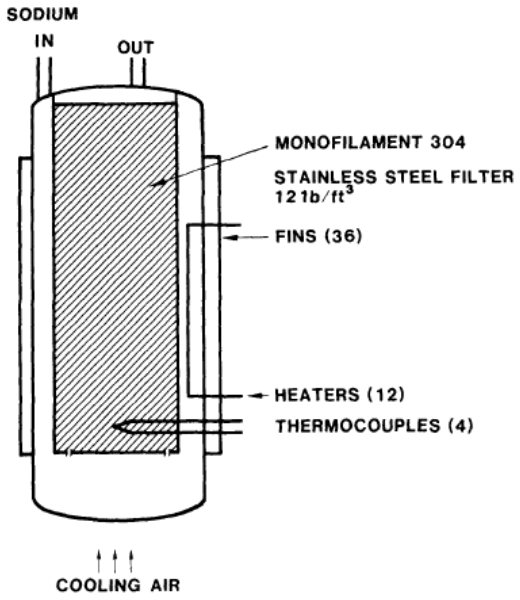

Figure 18: Cold trap conceptual sketch for a sodium loop [7].

2.3.2 NaK Centrifuging

The idea of this approach is to occasionally remove the NaK from the system and then centrifuge it at room temperature in an argon environment. The NaK is centrifuged in order to remove the heavier oxides. The argon environment allows the centrifuging to occur without the risk of fires or hydrogen build up. The closest similar research topic was on centrifuging high purity, melted gallium and then following solidification, analyzing the resulting crystal lattice structure and micro-hardness. The crystallized metal showed a small change in the lattice parameter and increasing micro-hardness with increasing acceleration in the centrifuge process due to plastic deformation upon cooling [14]. This unfortunately does not give any insight on the ability to remove impurities from

NaK using a centrifuge, since NaK would be difficult to solidify at room temperature. As such, investigating the feasibility of NaK centrifuging is an additional side topic that was evaluated.

The bench-top centrifuge test was performed to see if centrifuging the NaK was a practical option for maintaining low oxygen levels in an experimental setting. Due to the density difference between NaK and the oxides of sodium and potassium, this approach should work in theory. Sodium oxide has a density of 2.27g/cm^3 and potassium oxide has a density of 2.35 g/cm^3, while NaK has a density of 0.855 g/cm^3. The bench-top centrifuge test was performed in a sealed argon filled glove-box to limit additional oxide formation. When this test was performed the oxygen and water vapor levels in the box were each less than or equal 1ppm. The test was performed using the normal laboratory centrifuge show in figure 19.

The first centrifuge test was performed on NaK straight out of the shipping container and resulted in no visible separation of the NaK from any impurities. This was not a cause for concern, considering the NaK purchased was at least 99% pure. Due to the lack of visible separation, no quantitative measurements could be taken. It is relevant to note that the NaK was difficult to remove from the wall of the quartz centrifuge tube, and its high surface tension had it behave in a manner similar to mercury when pouring it back into the container.

The second centrifuge test was performed after allowing the NaK to sit overnight exposed to the argon atmosphere. It was believed that the exposure to a limited oxygen environment overnight would allow some sodium oxide and potassium oxide to form

without the danger of the potassium super-oxide forming. However, the surface of the NaK was not the white of the oxides or the yellow of the super-oxide; it was black. This black formation is most likely potassium nitride (black) and sodium nitride (reddish brown to dark blue). As such, the decision was made to centrifuge the NaK. This time the centrifuge process resulted in a separation of the black surface formation and the silvery NaK. However, the black surface substance was too solid to pipet or syringe off the NaK, and removing the NaK from the centrifuge tube still left a considerable amount of NaK adhered onto the walls of the tube. Thus, it was impossible to get a reliable mass measurement of the surface formation. The centrifuging method may still be practical with specialized equipment, but it is nearly impossible to perform with basic equipment.

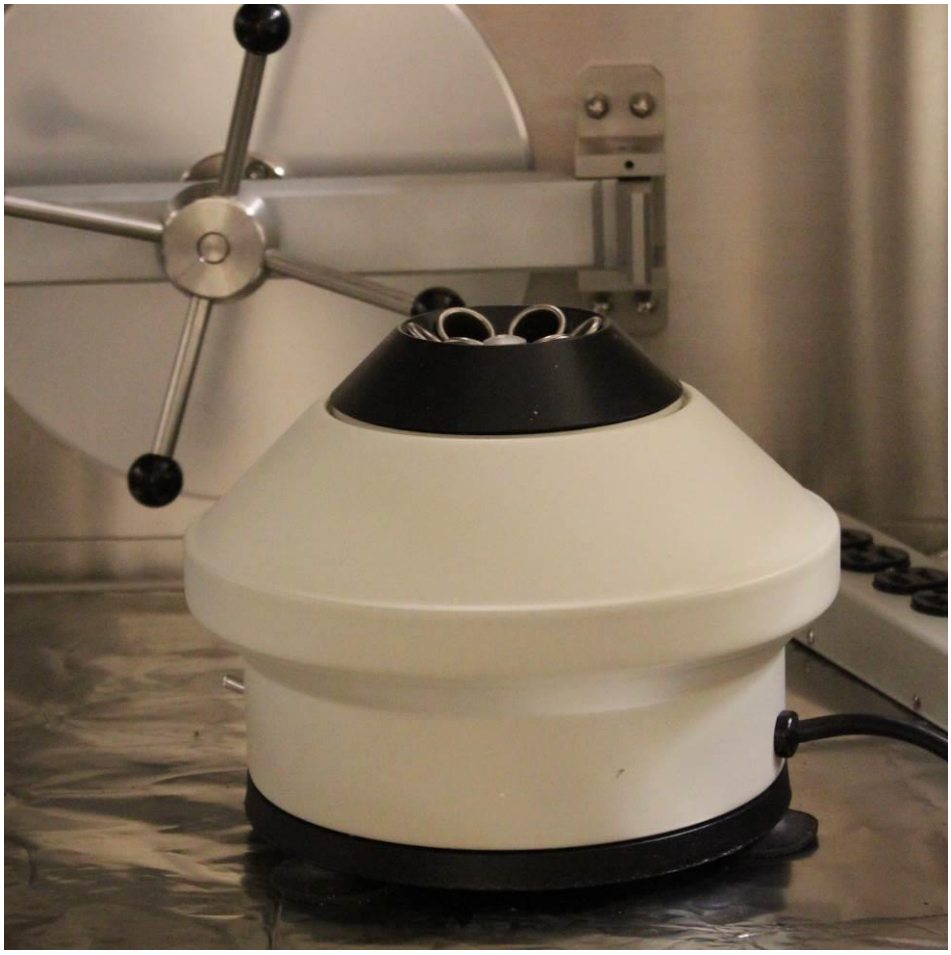

Figure 19: The centrifuge used on the NaK inside the glove-box.

Chapter 3

Design and Construction of the NaK Test Loop

3.1 Design of the Test Loop

3.1.1 Overall System Design

The overall design requirements for the system were continuous, long term operation, flowing NaK, sufficiently compact to fit in the glove-box, and capability of operating at 650°C. Several options were considered to generate flow in the system. One such option was an electromagnetic pump. An EM pump is usually an excellent way to drive NaK flow, but in this system EM pumps run into several difficulties. First, most EM pumps are fairly large, requiring coils, cooling systems, large ferromagnetic yokes, or motors for rotating magnet induction pumps. Also, downsizing an existing EM pump design for this test system leads to thinner gage wire, lower electrical load limits, and difficulty optimizing geometry. Mechanical pump designs were also considered, but ones that were robust enough for the operating environment would be difficult to fit into the glove-box. In addition, many standard mechanical pumps available would have NaK exposed surfaces that would melt or rapidly corrode in 650°C NaK. As such, a mechanical pump would to need be tailored to fit this specific situation. Thus, the choice was made to make the system's flow be driven by natural convection. To have effective, convective flow, the system needed a large temperature differential between the hot and cold legs. A furnace was considered sufficient to heat the hot leg. In order to further cool the cold leg a heat exchanger was used.

In order to operate for a long period at the 650°C, a proper material needed be used. The material choice was straightforward, with the test loop matching the material to be used in the NaK space reactor. The reactor this research project is being performed for utilizes 316L stainless steel as its heat exchanger and pipe material. Thus, nearly all test loop components are made from 316L SST. However, the test loop utilizes many standard vacuum fittings, including some that require gaskets. Zirconium, being softer than 316L SST, was chosen as the material for gaskets due to its resistance to corrosion by NaK [15].

This test loop was constructed with mostly standard parts and components. However, due to space restrictions and the use of NaK, several components for the system had to be custom made to adjust dimensions, assemble parts, or switch materials. Specifically, the gaskets used for Conflat* flanges, the specimen chamber/furnace, the expansion tank, and the dump tank were all adjusted to fit the space and material requirements. A Conflat junction uses two flanges each with a knife edge to cut into a gasket between the flanges by tightening bolts in order to create a vacuum seal. The tube junctions and valves were all standard Swagelok** components. All Swagelok junctions were 316L SST, and the high temperature NaK valves were Swagelok U-series, bellows-sealed valves, and the argon line valves were Swagelok 316L SST ball valves. In addition, sixteen K-type thermocouples were made to measure temperature behavior throughout the system. In figure 20, one can see the planned layout of the components used in the system and the general shape in which the stainless steel tubing is arranged.

*Conflat is a registered trademark of Varian, Inc.
**Swagelok is a registered trademark of the Swagelok Company

In addition, both a dump tank and an expansion tank needed to be custom made. An expansion tank was necessary due to the thermal expansion of NaK when heated, which leads to significant volume increases. A dump tank was necessary as both a loading tank for the NaK and a draining tank for when the weld specimens need to be removed. The approach used was to purchase two 22.9 cm (9 in.) diameter 316L stainless steel beakers. These beakers were cut 2.54 cm (1 in.) above the bottom for the expansion tank, and 7.62 cm (3 in.) above the bottom for the dump tank. Two plates and the cut beaker bottoms were then cut with the desired holes so that tubing could be welded onto the tanks. The cuts, welds, and the number of required holes and their rough postion can be inferred from figure 20.

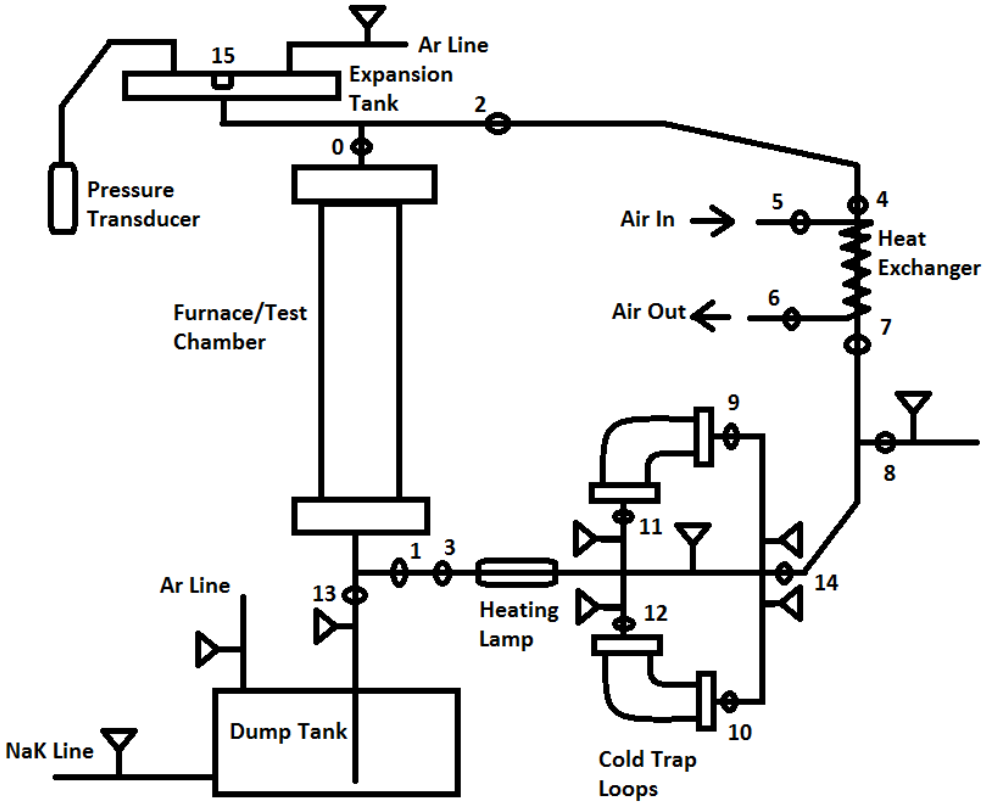

Figure 20: Diagram of the NaK test loop with components labeled. Note: both cold trap legs are below the lower horizontal leg.

3.2 Design and Construction of the Test Loop Components

The test loop was designed to fill several design requirements. The first requirement to be met was safely creating and operating a sample chamber with 650°C flowing NaK. To do this a furnace/sample chamber needed to be designed and made. Convective NaK flow required a cold leg heat exchanger to ensure a sufficient temperature differential. In order to address safety concerns for the university labs, the system needed to be in an inert atmosphere. In addition, a purification method needed to be added to maintain low oxygen levels in the NaK. Maintaining low oxygen levels is

the most effective means of controlling mass transfer in NaK loop, which is the major source of stainless steel corrosion in a NaK loop [15]. Zirconium corrosion in NaK is also oxygen dependent, since the formation of an oxide-film will act as a crack initiator in a fatigue situation [15]. Finally, a method to measure or at least verify NaK flow needed to be implemented to ensure that the NaK flow requirement was met.

3.2.1 Purification Loop: Cold Traps

When working with NaK, cold traps are the most common method of reducing oxygen levels. NaK cold traps work on the basic principle of cooling the liquid metal down to reduce the solubility of oxygen causing it to precipitate as an oxide. These oxides are removed from the flowing liquid by running the liquid through a trap of steel filament mesh. The goal was to construct a simple purification loop that would not greatly reduce flow and be large enough to not be clogged after long term use. The cold trap was designed to operate in line with the flow instead of creating a specialized tank as done in many applications [15]. Also, to remove the chance of the cold trap stopping flow, two independent cold trap loops were included in the design as seen in figure 21. Finally, two thermocouples were included on each cold trap loop in order to allow a temperature measurement to be taken, so that the NaK solubility level in the trap could be predicted.

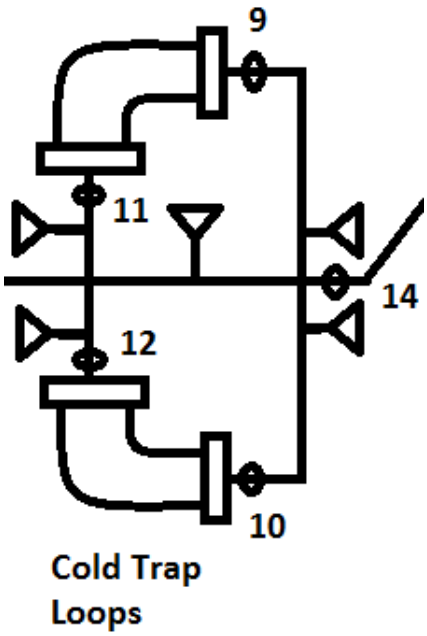

Figure 21: Two independent cold trap loops with a bypass option.

The cold traps were constructed using off the shelf standard parts. The trap was created using two Conflat blank flanges, a Conflat 90° bend component, and 316L stainless steel wool. Each blank flange had a nominal 6.4 mm (¼ in.) bore drilled into the center of the flange 2/3 of the way through the flange. A 5.8 mm (0.23 in.) diameter hole was then drilled through the center of the bore to create a lip. A 6.4 mm (¼ in.) tube was then inserted into each flange until it bottomed out on the lip. Each tube and flange pair was then welded using a gas tungsten arc welder. Figure 22 provides a view at the fully completed flange with the recess weld viewable.

Special metal gaskets resistant to NaK had to be made. There were two material choices considered for the gaskets, niobium and zirconium, since the standard copper gaskets would be quickly corroded by the high temperature, flowing NaK. In terms of

corrosion resistance, zirconium and niobium are quite similar, thus the decision to use zirconium was based on accessibility, instead of any perceived advantage.

At this stage all the cold trap components were created and the assembly could be performed. Figure 23 shows the Conflat 90° bend component filled with the 316L stainless steel wool used to trap oxides. The final assembly of the cold trap can be seen in figure 24.

Figure 22: The cold trap flanges were created using a .64 cm (1/4 in.) diameter tube and welding it to the flange.

Figure 23: The 90° bend component with the stainless steel wool inside.

Figure 24: The assembly of the cold trap.

3.2.2 Heat Exchanger

A heat exchanger was a necessary component in the system due to the decision to utilize convective flow. Convective flow is driven by pressure changes resulting from density changes caused by temperature differential. The heat exchanger was needed to create a large temperature differential between the hot and cold legs, which causes a

significant difference in density between the two legs. These different densities cause a pressure difference leading to fluid flow.

Three standard heat exchangers were considered for this loop. The first considered was a tube-plate heat exchanger. The second heat exchanger considered was a spiral heat exchanger. Lastly, a simple coil heat exchanger was also analyzed for use in this loop. All three options were to be air cooled using a compressor to drive air flow. Of the three options, the coil heat exchanger is the least efficient, compared to the other options. However, a coil heat exchanger provides a double boundary between the NaK and the cooling air, while the tube-plate and spiral heat exchangers provide only one. This was particularly advantageous, since a failure in the heat exchanger could potentially be dangerous due to NaK's reactivity with air. Thus, a coil exchanger was chosen for long term survivability, and a double tube wall redundancy separating the NaK and coolant (air). The coil heat exchanger made comprised of a small diameter tube wrapped around a larger diameter tube containing the NaK.

The coil heat exchanger was created using soft copper 6.4 mm (¼ in.) tubing of 3.05 meters (10 ft.) in length. In order to wrap the copper tubing around the 1.27 cm (½ in.) steel tubing, the copper tubing had to be filled with sand in order to prevent crimping of the tube. After filling it with sand, the ends of the tubing were pre-crimped to compress the sand. Then the tubing was wrapped around a 1.27 cm (½ in.) steel rod. The coil heat exchanger was then slid off the rod. The sand was then removed from the copper tubing by blowing compressed air through the tubing. Next the stainless steel

tubing was coated with thermal cement. Finally, the coil heat exchanger was slid onto the 1.27 cm (½ in.) tubing.

There were several iterations of the coil heat exchanger made due to issues with the copper tubing severely crimping on the first or second wrap. One such iteration can be seen in figure 25. This issue was solved when the pre-crimping step was added. By crushing about 1 to 2 inches on each side the tubing and later cutting off the ends, there was no difficultly with the copper crimping and potentially blocking flow.

Figure 25: One iteration of the coil heat exchanger where the copper was severely crimped.

3.2.3 Furnace/Specimen Chamber

The specimen chamber was designed with several requirements in mind. The first requirement was to expose the maximum number of samples to 650°C NaK. The next requirement was to maintain a uniform temperature profile for the samples. Third, the system needed to be accessed and samples removed while inside the glove-box. In order to help achieve all three of these objectives, the decision to combine the furnace and the specimen chamber was made. By combining the two in a single unit, it reduced the height of the system by not having both a heater and a sample chamber on the hot leg of the loop. This permitted a large sample chamber, with a height of 22.9 cm (9 in.) and an outer diameter of 6.4 cm (2.5 in.) with an internal volume of about 800 cm^3. The sample chamber pipe was welded to two Conflat flanges so that it can be readily attached or detached from the rest of the system. In addition, five thermocouple wells were originally intended to enter into the specimen chamber to measure the NaK temperature at varying heights throughout the specimen chamber. These wells, shown in figure 26, were later removed from the design; since they would interfere with specimen loading. In addition, the furnace had six thermocouples at varying heights on the outside of the chamber for temperature control, making the wells a redundant feature.

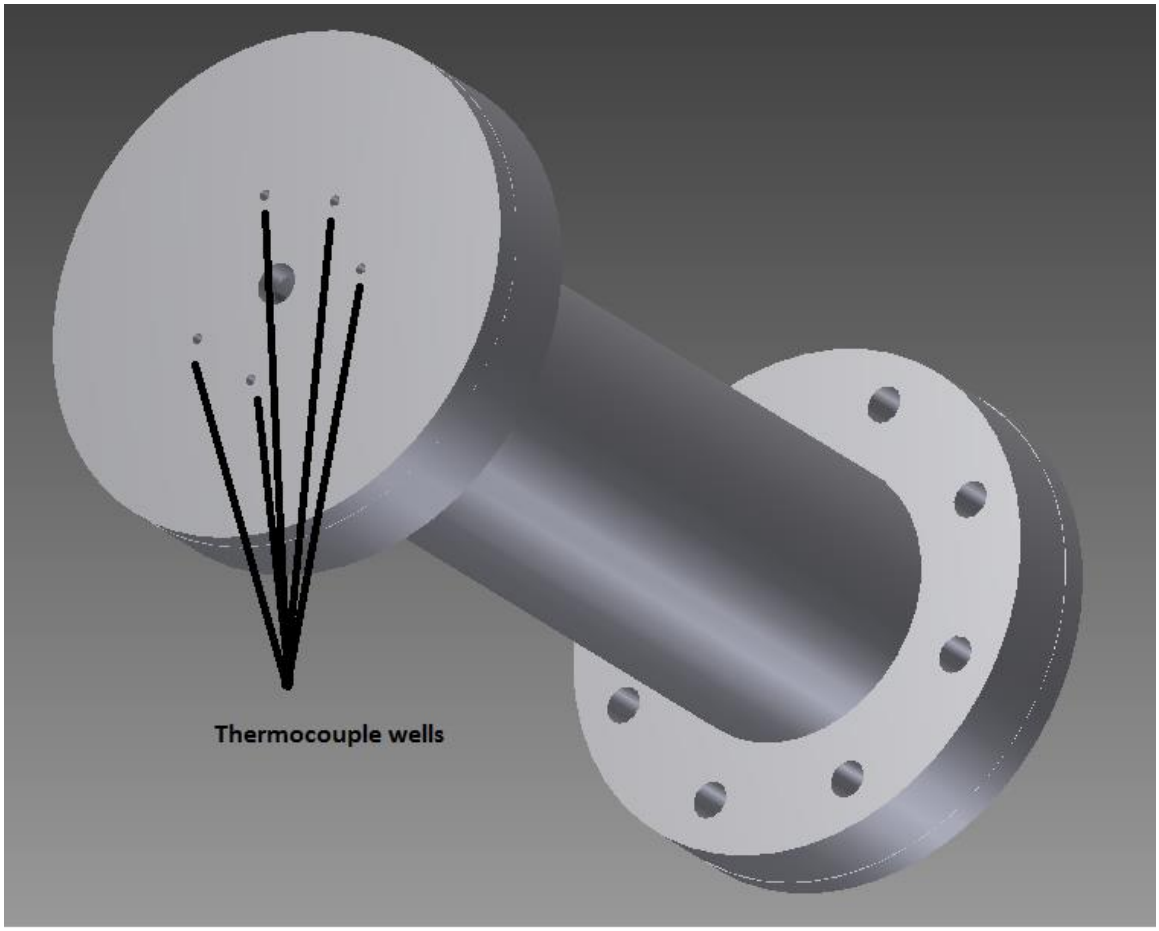

*Figure 26: Model of the heater/specimen chamber. *Note the outer flanges on the model do not show the bolt holes.*

The furnace/specimen chamber was constructed in a manner quite similar to the cold traps. The main body of the chamber was a 6.35 cm (2.5 in.) outer diameter tube that was 27.94 cm (11 in.) in length. The chamber tube was welded to a Conflat flange on each end. The assembly had a three zone furnace wound around it. The furnace has two shorter coils at each end of the chamber tube, and one larger coil in the center of the chamber tube. Prior to loading specimens, the loop needed to be tested. Thus, this time

the chamber was assembled without the specimen rack. To finish the assembly, two blank Conflat flanges needed to be drilled and welded to 1.27 cm (½ in.) tubes. In addition, the custom zirconium gaskets for the chamber were also machined. Figure 27 shows a fully assembled furnace/specimen chamber with the insulation pulled back to show the three zone heating coils.

Figure 27: The assembled furnace/specimen chamber with the heating coils exposed.

3.2.4 Specimen Rack

The specimen rack's design focused on maximizing the number of samples without restricting NaK flow. First, the rack needed to be able to fit inside the specimen chamber. In addition, it needed to hold a total of 64 samples so that all the candidate weld samples could be exposed simultaneously. Finally, the specimen rack needed to not overtly obstruct NaK flow through the specimen chamber.

The rack consisted of eight plates held together by five threaded rods. Each plate contained a heptagonal circular arrangement of 1 cm (.4 in) holes and one additional 1 cm (.4 in) hole in the center to hold a total of eight samples on each plate. Also, each plate contained another heptagonal set of smaller holes for the supporting rods, as shown in figure 28. The outer diameter of each plate was 5.1 cm (2 in.), which was smaller than the inner diameter 6.03 cm (2.38 in.) of the specimen chamber to insure NaK could flow freely around the rack. The details of the plates can be seen in figure 29. Figure 30 shows an assembled specimen rack.

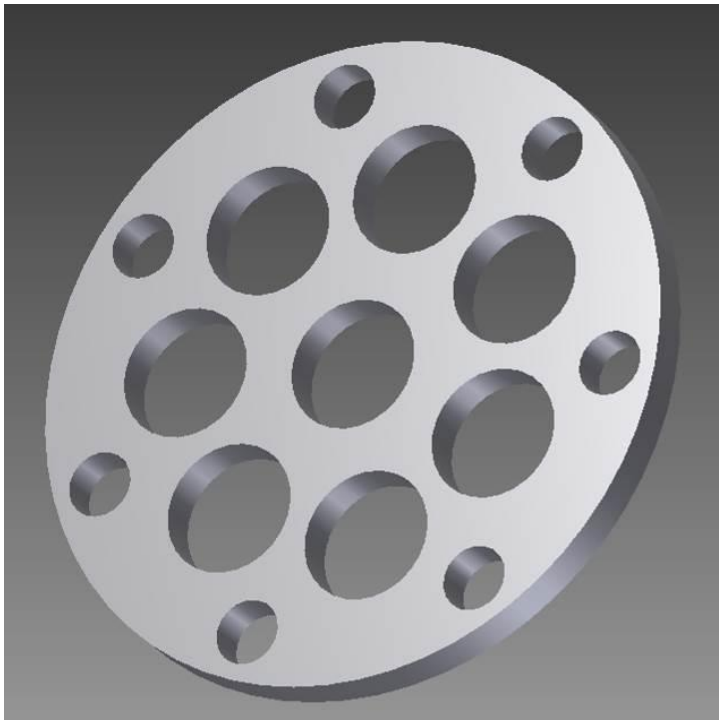

Figure 28: Model of one of the eight plates to be used to construct specimen rack.

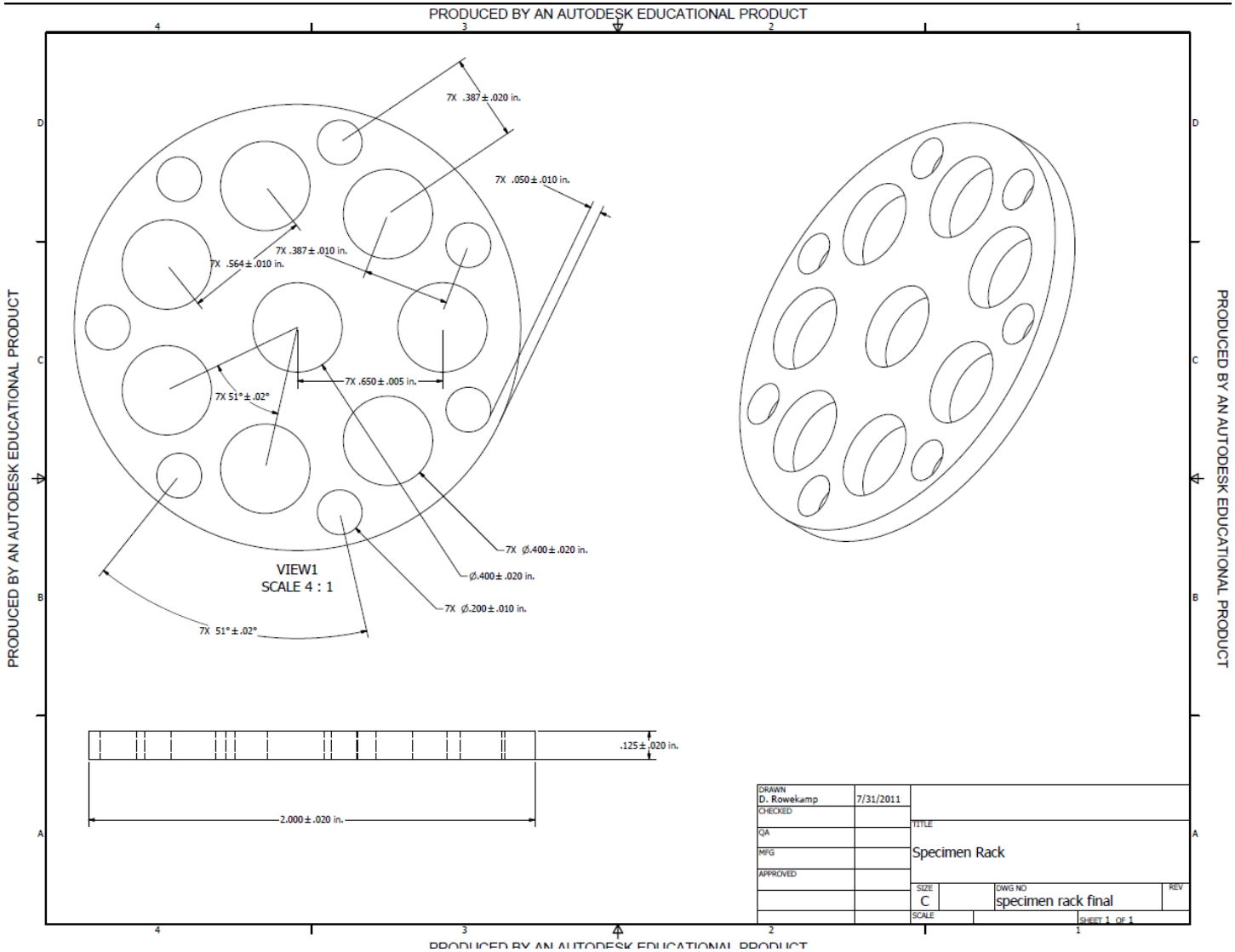

Figure 29: CAD drawing of the specimen plate.

Figure 30: The finished specimen rack with some samples removed to highlight the structure of the rack.

3.2.5 System Assembly

The full system assembly was fairly straight forward. Most of the work comprised attaching the prevously mentioned components together using standard swagelok fittings and pieces of stainless steel tubing. However, a pressure transducer

was needed to measure the pressure in the system, since a sharp pressure increase would be a good indicator of boiling NaK. Thus, an Ashcroft DXD* pressure transducer was purchased. This transducer was attached to the expansion tank by a long tube to separate it as far as possible from the high temperature furnace. Finally, the fully assembled system inside the glove-box can be seen in figure 31.

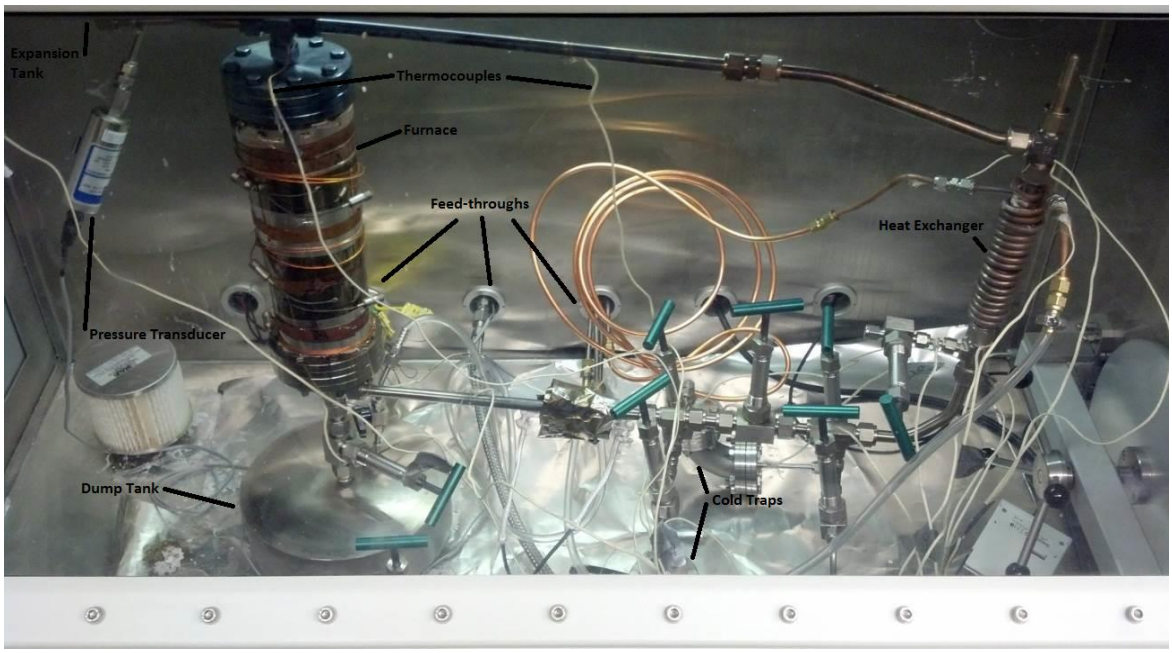

*Figure 31: The fully assembled system in an argon filled glove-box. In this picture the system is fully attached to all necessary external feedthroughs. *Note that system does not have its insulation attached in this picture.*

*The pressure transducer used for this research project, was a digital pressure transducer purchased from Ashcroft®.

Chapter 4

System Testing and Flow Velocity Measurement

4.1 Convective Flow Confirmation Test

A helium leak test was performed on the system, and the system was made leak tight. The system was tested to verify the presence of convective flow. NaK flow was confirmed by analyzing the behavior of thermocouples 0, 1, and 2, whose positions are shown in figure 32. If convective flow begins as the temperature is raised, there should be a sharp increase in temperature in thermocouples 0 and 2, and a decrease in thermocouple 1 as convective flow becomes dominant over the conductive heat transfer. This behavior can be viewed in Figure 33, where the temperatures of thermocouples 0, 1, and 2 are plotted against time as the furnace was heated from room temperature to 250°C. Thus, significant convective flow was detected as the furnace reached approximately 250°C. The behavior of thermocouple 1 indicates that the occurring convective flow was sufficient to overcome the conductive heat transfer in the NaK.

The temperature measurements were taken using K-type thermocouples attached to a National Instruments DAQ card*. The DAQ card was connected to a computer and the data was collected using LabView** software. Temperatures were logged at each thermocouple every second for the duration of this test.

*The NI USB-9213 DAQ card is National Instruments product.
** LabView is a software package and registered trademark of National Instruments.

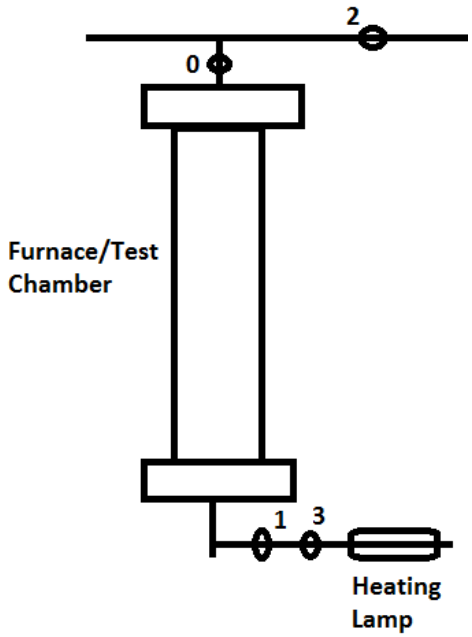

Figure 32: Diagram showing the layout of the thermocouples used to confirm convective flow.

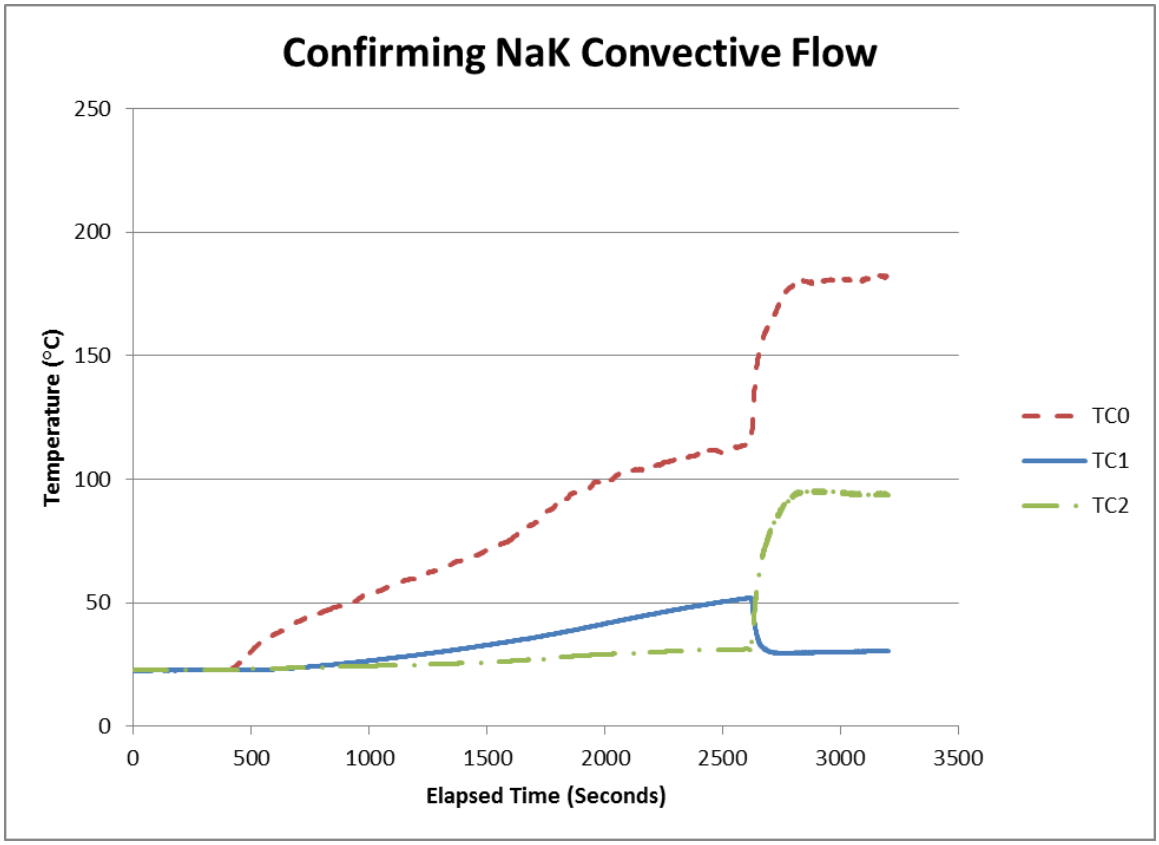

Figure 33: Temperature behavior at thermocouples 0, 1, and 2, which confirms NaK convective flow has started as the temperature of thermocouple 1 drops as the system is heated further.

4.2 Flow Measurement: Heat Spike Tracing

One of the requirements for the test loop was that the NaK needed to be flowing to simulate space reactor conditions. Thus, a method to measure or at least detect the flow of NaK was necessary. Several approaches were considered as potential options for this need. The standard approaches considered were a Venturi flow meter and an electromagnetic flow meter. A commercially available Venturi flow meter capable of withstanding 650°C was not available. Specifically, it was a challenge to find an

available meter that was all 316L stainless steel. The EM flow meters and sensors were also considered; however, most available were not rated for the high temperature NaK in this loop. Thus, the decision was made to use the heat spike method used by Tortorelli [10]. However, a torch could not be used due to the argon environment, thus a different heating approach was needed. The method chosen was to use a 500W lamp to heat the NaK. This lamp could be turned on and off with a switch to generate a heat spike. A simple diagram showing the location and orientation of the heating lamp and the thermocouples used to detect the spike can be seen in figure 34.

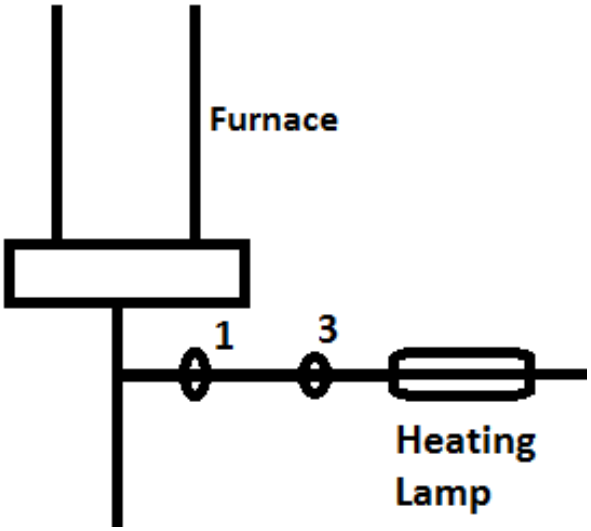

Figure 34: Diagram showing the orientation of the heating lamp, thermocouples 1 and 3, and the bottom of the heater/specimen chamber.

The heat spike system is comprised of three major components, two K-type thermocouples and a 500W quartz heating lamp that is used to generate the heat spike. The lamp was wrapped in stainless steel foil to reflect the intense light towards the tubing. Figure 35 shows the all the components of the heat spike tracing system.

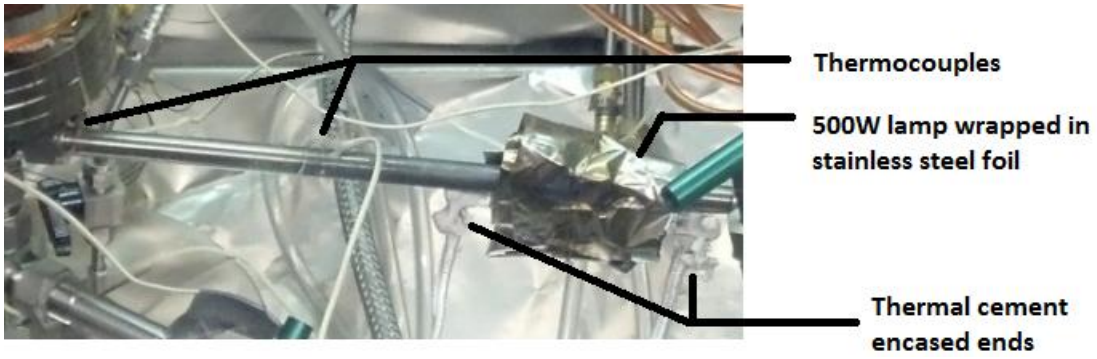

Figure 35: The heat spike tracing system attached to the assembled system.

Measuring the flow velocity of the NaK by tracing a heat spike requires a couple simple steps. First, the heat spike needs to be applied. The loop was heated by a 500W quartz lamp lashed to the system for 5 seconds for each trial. The temperatures at the relevant thermcouples need to be plotted so the time when the heat spike passed can be evaluated. As an example the two spikes for trial 11 can be seen in Figure 36, and all trials can be seen in the appendix A. Measuring the x-axis between the two heat spike detections gives the time to travel between the two thermocouples. Also, a simple measurement of the distance between the two thermocouples gives the distance traveled by the heat spike. Now the velocity of the heat spike can be calculated.

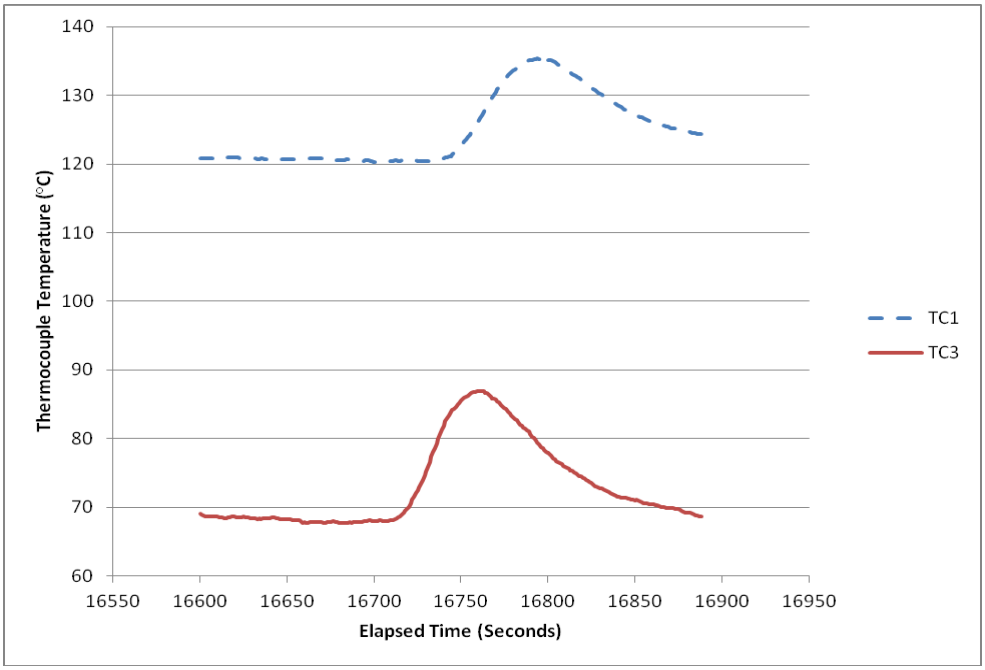

Figure 36: The heat spike passing thermocouples 1 and 3 for Trial 11.

A difficulty experienced was determining when a spike reached the thermcouple. In order to determine when the spike arrived, two different methods were performed. The first method worked by measuring the time from peak to peak. The second method was performed by measuring the time from the start of each peak. A side by side comparison of the two methods for eleven trials can be seen in figure 37.

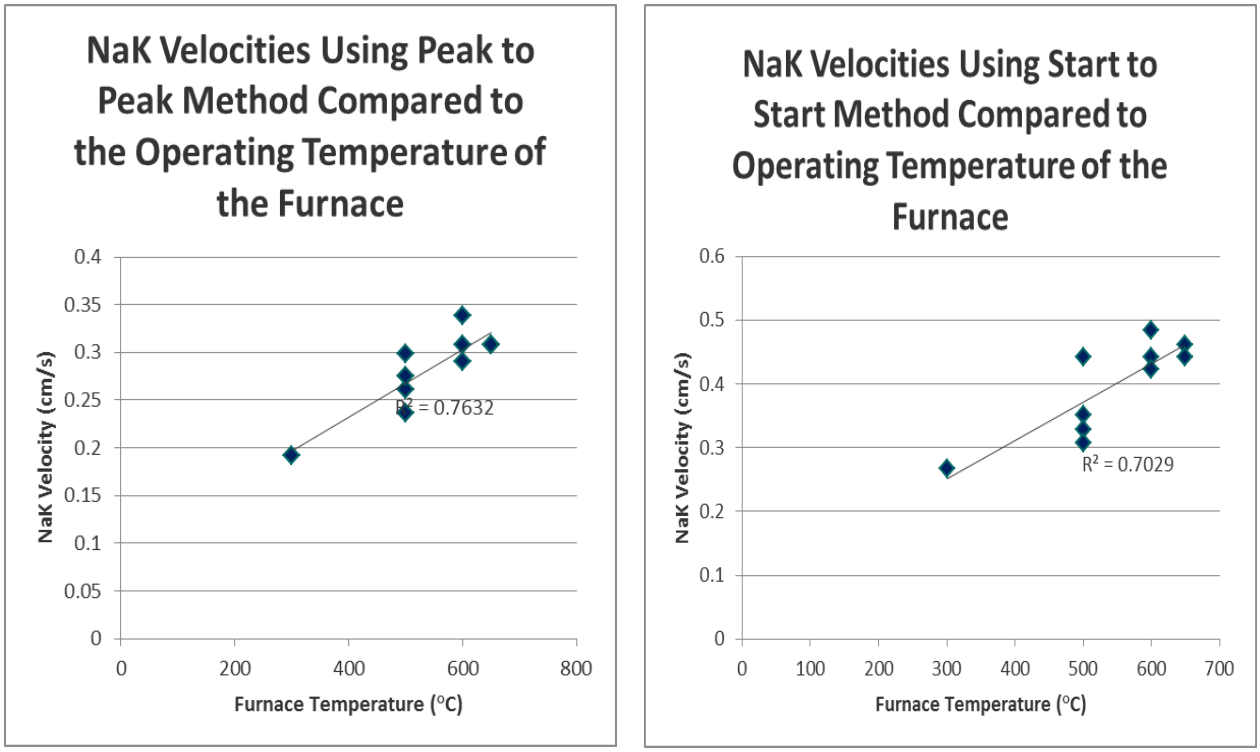

Figure 37: Comparison of the two methods used to measure the travel time between two thermocouples for the hot slug of NaK created from the heat spike. Data is graphed with NaK velocity being a function of furnace temperature.

The start to start method gave higher velocities across the all trials compared to the velocities of the peak to peak method. This is likely due the conductive heat transfer spreading heat from the spike forward and behind the hot slug of NaK. From the correlation factor, the peak to peak method has more tightly clustered data, indicating a method with a higher precision. In additon to higher precision, the peak should still occur when the hottest NaK reaches the thermocouples, and the hottest NaK should typically be in the center of the hot slug. As such, the peak to peak method is likely more

accurate than start to start method. The results for the peak to peak method for all eleven trials are shown in Table 3.

Table 3: Furnace Temperatures and NaK Thermal Convection Flow Velocities.

Funace Temp.	**Avg. Cold Leg Temp.**	**Hot Leg-Cold Leg**	**Flow Velocity**
°C	**°C**	**°C**	**mm/s**
300	72	228	1.9
500	102	398	2.6
500	109	391	3
500	104	396	2.7
500	97	403	2.4
600	130	470	3.4
600	125	475	2.9
600	120	480	3.1
650	129	521	3.1
650	125	525	3.1

Figure 38 shows the measured NaK velocities as a function of the temperature differential between the furnace and the average temperature in the cold leg heat exchanger. This graph is somewhat more meaningful than the previous velocity graphs, since temperature differential is the driving force behind convective flow. Comparing figures 38 and 39, the differential temperature varies in a similar manner as the furnace temperature. As one expects, the general behavior of the data is the same in both plots, with the data forming roughly the same clusters in both. However, the temperature differential graph accounts for temperature instability in the heat exchanger, since it uses the temperature differential in the system and not the set furnace temperature. As such the temperature differential graph is the more realistic model. The temperature

differential values use the measurements of the average temperature of the cold leg which were found by averaging the temperatures of thermocouples 4 and 7, and subtracting that average from the furnace temperature.

A notable difficulty experienced early in the measurements was that the lamp perturbed the NaK flow. The hot NaK slug appeared to increase the flow velocity as it traversed the furnace, leading to a higher velocity measurement. In addition, at 400°C, flow instability resulted in temperature oscillations. To correct the perturbation problem, temperature measurements were made between two thermocouples in the bottom segment of the loop. In this way, the measurements were complete before the hot slug of NaK reached the vertical segment of the loop. A disadvantage to this method was loss of precision in using a short length of pipe. Despite this improvement in the measurement technique, instabilities were still experienced at 400°C.

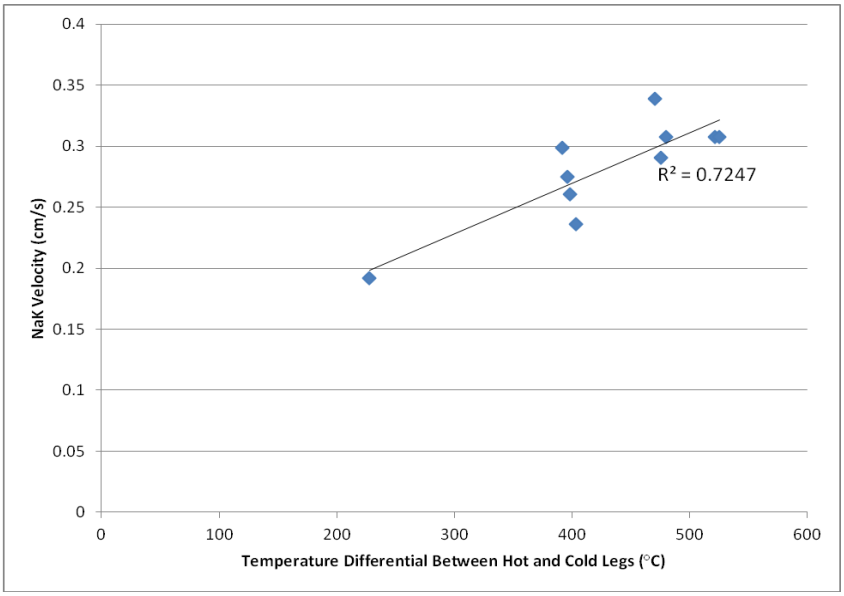

Figure 38: Plot of the NaK velocity as a function of the hot and cold leg temperature differential.

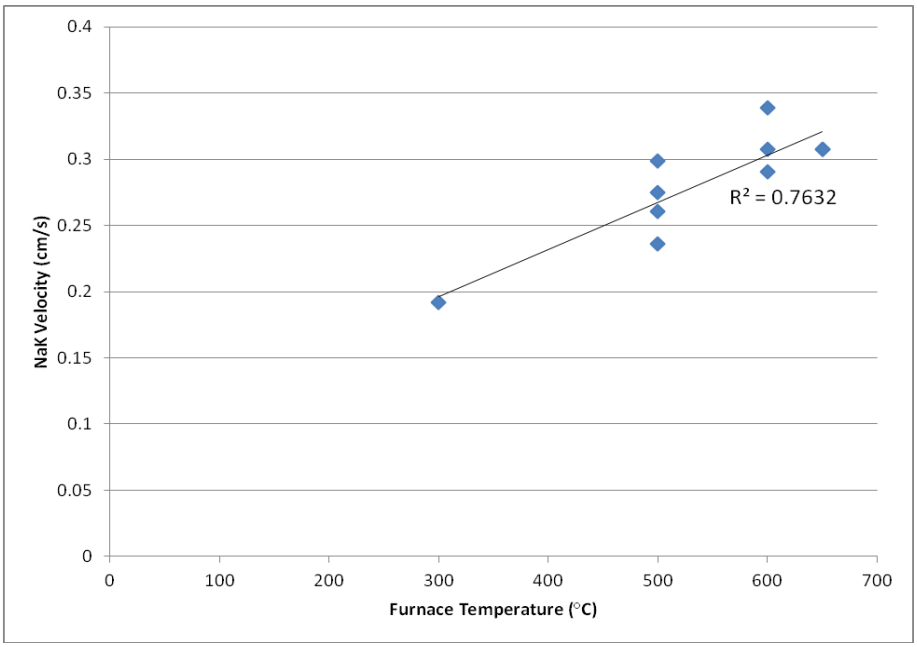

Figure 39: Plot of the NaK velocity as a function of the furnace temperature.

A thermal convection lithium loop was studied by Tortorelli and DeVan where fluid velocity was measured by a somewhat similar technique [10]. Comparison to Tortorelli and DeVan's Li loop results showed a lower flow rate of NaK than of Li for even higher differential temperatures. The lithium loop showed a velocity of approximately 30 mm/s whereas the maximum velocity of the NaK loop was found to be 3 mm/s [10]. At least part of this discrepancy could be due to the longer hot and cold segments of the lithium loop. However, based upon the thermal expansion coefficients of the two materials and the longer lithium loop, the lithium would be expected to have about a 12% higher velocity. This 12% estimate was calculated proportionally as follows:

$\rho_{NaK}(200°C) = .825\ g/cm^3$ $\qquad$ $\rho_{Li}(300°C) = .505\ g/cm^3$

$\rho_{NaK}(350°C) = .790\ g/cm^3$ $\qquad$ $\rho_{Li}(450°C) = .490\ g/cm^3$

$\Delta\rho_{NaK} = .035\ g/cm^3$ $\qquad$ $\Delta\rho_{Li} = .015\ g/cm^3$

NaK loop hot leg length = 29.2cm $\qquad$ Li loop hot leg length = 76cm

$Force \propto \Delta m * g * l \propto l * \Delta p$ $\qquad$ $\frac{l * \Delta\rho_{Li}}{l * \Delta\rho_{NaK}} = \frac{1.14 g/cm^2}{1.02 g/cm^2} = 1.12$

Differences in flow resistance of the two loops could be a major factor in the variation, but it is also possible that the lithium loop velocity was influenced by perturbation of flow by the torch heating of the loop to make the velocity measurements. Also, the Li loop was 76.2 cm (2.5 ft.) in height and less than 15.2 cm (0.5 ft.) in width, while this loop is 30.5 cm (1 ft.) in height, and nearly 91.4 cm (3 ft.) in width. The stoutness of this

loop could play a factor in the differing results. In addition, differences in insulation could play a major role in the noticeable difference between the two loops.

A hand calculation of the expected NaK flow rate was performed for when the system is fully insulated. This calculation can be viewed in the appendix B. The calculation utilizes several assumptions, such as negligible heat loss except at the heat exchanger, no flow loss at elbows, turbulent flow, and steady state flow. The calculation gives an expected axial flow velocity of 78.6 mm/sec in tubing for the assumptions above. Any actual flow would be less due to the assumptions used. This indicates that the 3 mm/sec flow measured in the NaK loop most likely stems from the lack of insulation. This might also explain the difference between the flow rate in the lithium loop and the NaK loop.

An additional concern was raised and investigated regarding the heat spike tracing method. The concern was whether the method measured conductive heat transfer or convective heat transfer from the NaK. As such, two additional trials of the heat spike tracing method were conducted with the furnace set to 300°C. In the first trial all valves on the cold trap loops and the cold trap bypass valve were closed. This configuration makes convective flow impossible and the resulting heat spike can be seen in figure 40. The second trial had the bypass valve open, so convective flow was possible. The resulting heat spike for the second trial can be seen in figure 41. The heat spike in the trial with the valves closed, took several times longer to reach thermocouples 3 and 1, respectively, than the heat spike in the open valve trial. This indicates that the heat spike

detected in the previous trials were not conduction peaks, and were in fact created by detecting the hot slug of NaK passing the thermocouples due to convective flow.

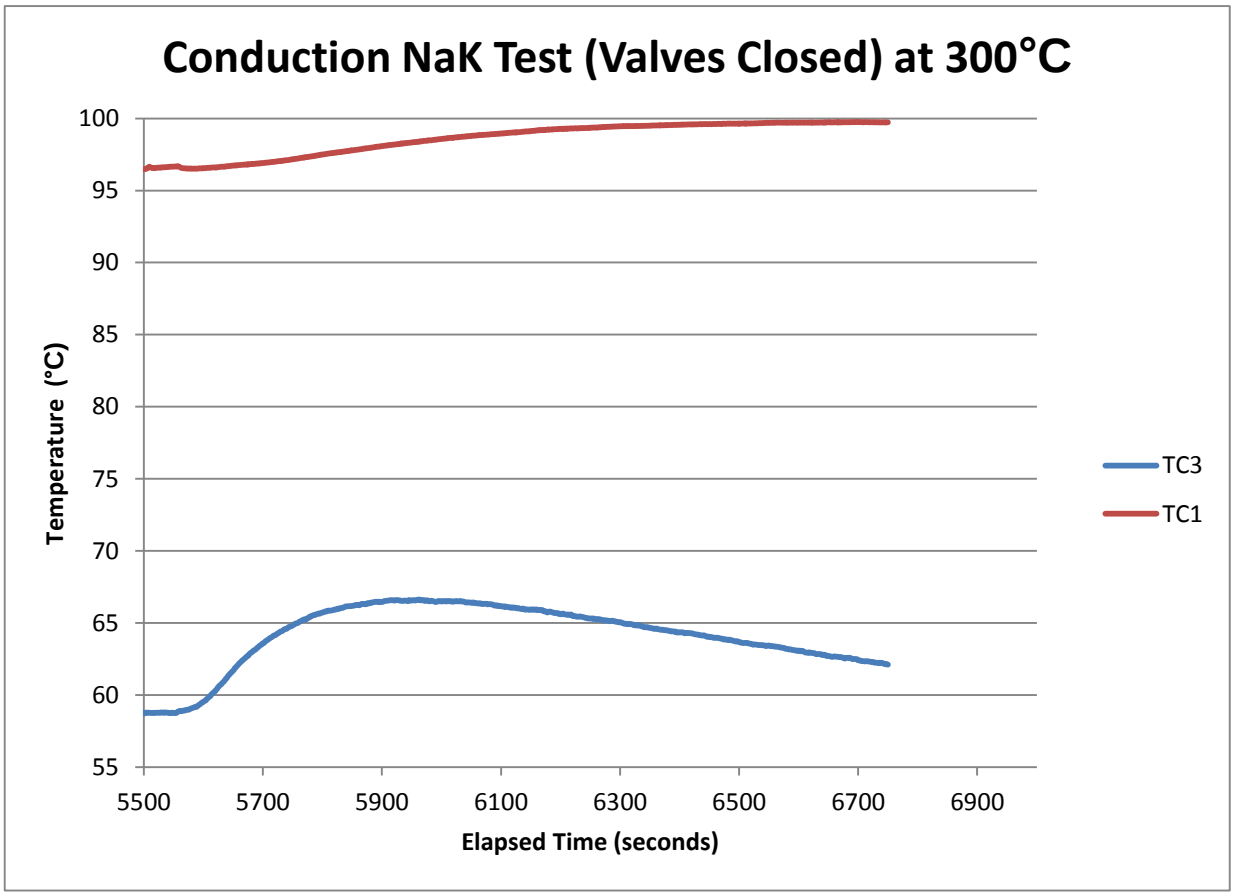

Figure 40: The results of the heat spike test with all valves closed.

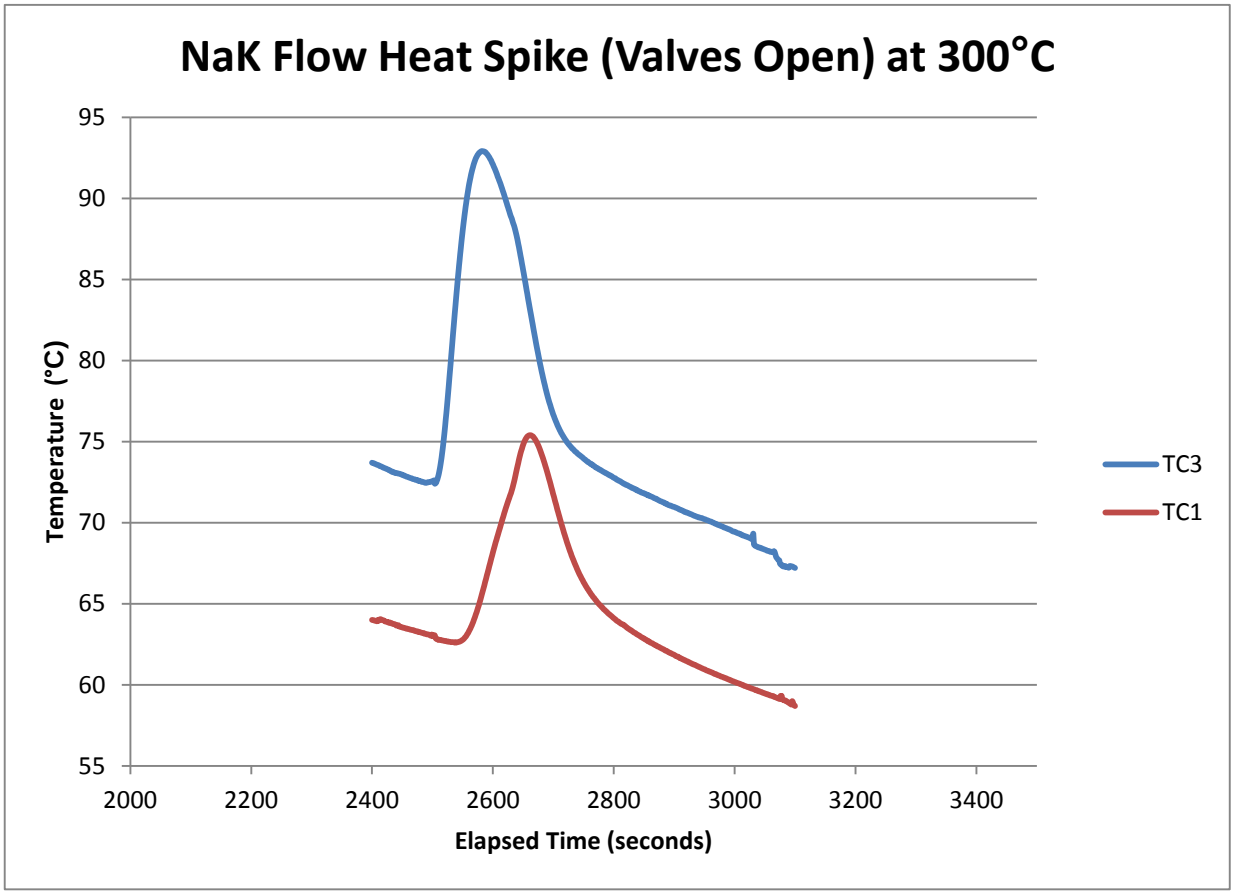

Figure 41: The results of the heat spike test with the cold trap loops' bypass valve open.

Chapter 5

Conclusions

A working NaK loop with convectively driven flow was successfully constructed and operated. The NaK loop successfully operated at 650°C. The heat spike tracing method of flow measurement showed potential as a safe, indirect way of determining flow velocity in NaK. The flow velocity in the system was not as high as expected, but the current lack of insulation and several factors in terms of loop geometry could have played a role. However, a flow velocity of 3 mm/s or a volumetric flow rate of 0.4 cm^3/s was achieved at the targeted operating temperature of 650°C. As such, the research project will advance onto the next stage of inserting the weld samples for exposure.

There are several recommendations for future work on the test system itself. A useful continuation would be to see a side by comparison of Venturi flow meter and the heat spike tracing method, or a comparison of a calibrated EM flow meter and the heat spike tracing method in the liquid metal loop. Also, repeating the heat spike tracing method testing once samples are added would be an excellent way to how much the filled specimen rack would obstruct flow in the system. Finally, the cold trap efficiency could be tested by running the loop without the cold traps and sampling the NaK, followed by running the system with the cold traps included and sampling the NaK in order to determine their effect on the ppm levels in the NaK.

List of References

1. T. Malkow, H. Steiner, H. Muscher *, J. Konys. "Mass transfer of iron impurities in LBE loops under non-isothermal flow conditions." *Journal of Nuclear Materials*. Vol. 335 (2004) 199–203. Elsevier
2. T. Cochran, H. Feiveson, W. Patterson, G. Pshakin, M. Ramana, M. Schneider, T. Suzuki, F. Hippel. "Fast Breeder Reactor Programs:History and Status." *International Panel on Fissile Materials February 2010*. Research Report 8
3. D. S. Armstrong. "Electro-Magnetic Pumps for Liquid Metals." *Students' Quarterly Journal*. September 1962. (51-59)
4. A. H. Barnes. "Direct-Current Electromagnetic Pumps." *Nucleonics.* Vol. 11, January 1953. (16-21)
5. K. A. Polzin. *Liquid-Metal Pump Technologies for Nuclear Surface Power.* NASA March 2007. NASA/TM-2007-214851.
6. I.N. Sviatoslavsky and E.A. Mogahed. "Design of Vertical Stabilizing Shells and Tutorial on EM Pumps." *ARIES Review Meeting*. June 19-21, 2000. University of Wisconsin Fusion Technology Institute.
7. R. Acton, R. Weatherbee, L. Smith, F. Mastin, K. Nowotny. *Sandia Sodium Purification Loop (SNAPL) Description and Operations Manual.* Sandia National Laboratories. August 1985. SAND84-0763.
8. T. Ando, K. Ueno, S. Taniguchi, and T. Takagi. "Induction Pump for High-Temperature Molten Metals Using Rotating Twisted Magnetic Field: Molten Gallium Experiment." *IEEE Transactions on Magnetics*, Vol. 40, No. 4, July 2004. (1848-1857)
9. I. Bucenieks, J. Freibergs, E. Platacis. "Evaluation of Parameters of Powerful Electromagnetic Induction Pumps on Permanent Magnets for Heavy Liquid Metals." *IV International Workshop on Materials for HLM-cooled Reactors and Related Technologies.* ROMA, ITALY, May 21-23, 2007. University of Latvia Institute of Physics.
10. P. Tortorelli and J. DeVan. "Thermal-Gradient Mass Transfer in Lithium-Stainless Steel Systems." *Journal of Nuclear Material.* Vol. 85-86. December 2, 1979. (289-293)
11. F. Wolf, C. Beckerman, and R. Viskanta. "Natural Convection of Liquid Metals in Vertical Cavities." *Experimental Thermal and Fluid Science*. 1988. (83-91)
12. "Venturi Flowmeter." http://hyperphysics.phy-astr.gsu.edu/hbase/fluids/venturi.html. Nov. 18, 2012.
13. T. Sakai, M. Gunji, S. Matsumoto, and Y. Ishii. "Determination of Oxygen Solubility in NaK-78 by Vacuum Distillation Method." *Journal of Nuclear Science and Technology.* Vol. 20. December 1983. (1032-1038)
14. V. Gurin, L. Derkachenko, I. Zimkin, M. Korsukova, and S. Nikanorov. "Centrifugation of Liquid Low-Melting Metals." *Technical Physics Letters*. Vol. 28. 2002. (162–163)

15. O. Foust. *Sodium-NaK Engineering Handbook.* Vol. 5. Gordon and Breach. 1972.
16. D.I. Poston, R. Kapernick, D. Dixon, J. Werner, L. Qualls, and R. Radel. "Reference Reactor Module Design for NASA's Lunar Fission Surface Power System." *Proc. Nuclear and Emerging Technologies for Space 2990, Atlanta, GA, June 14-19.* Paper 208589.

Appendices

Appendix A

The appendix A contains the NaK flow calculation and all the individual heat spike graphs for all 10 trials with the furnace temperature the trial was performed at stated on each graph. Note Trial 2 was omitted due flow oscillations preventing a steady state in the system. Also, Trial 11 is shown in figure 36.

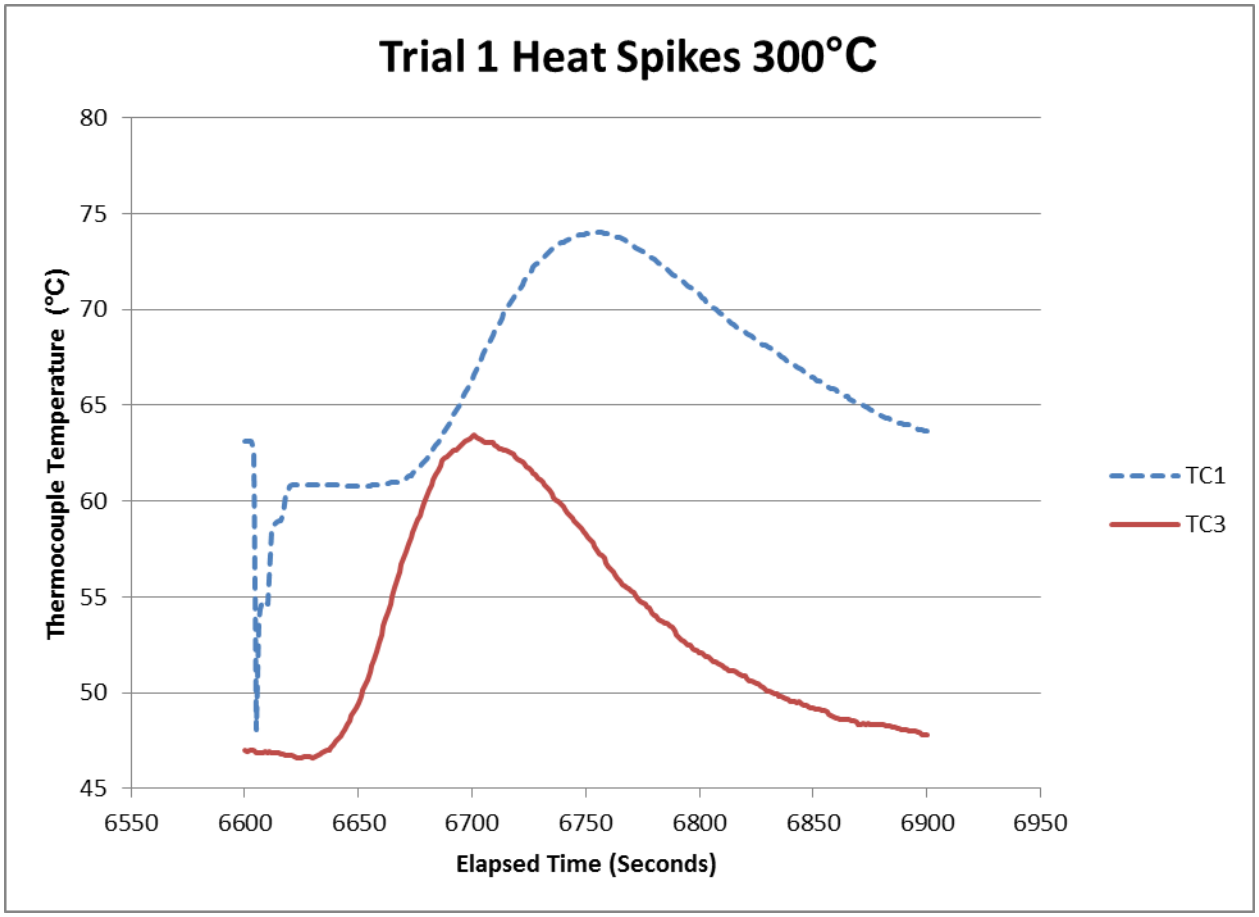

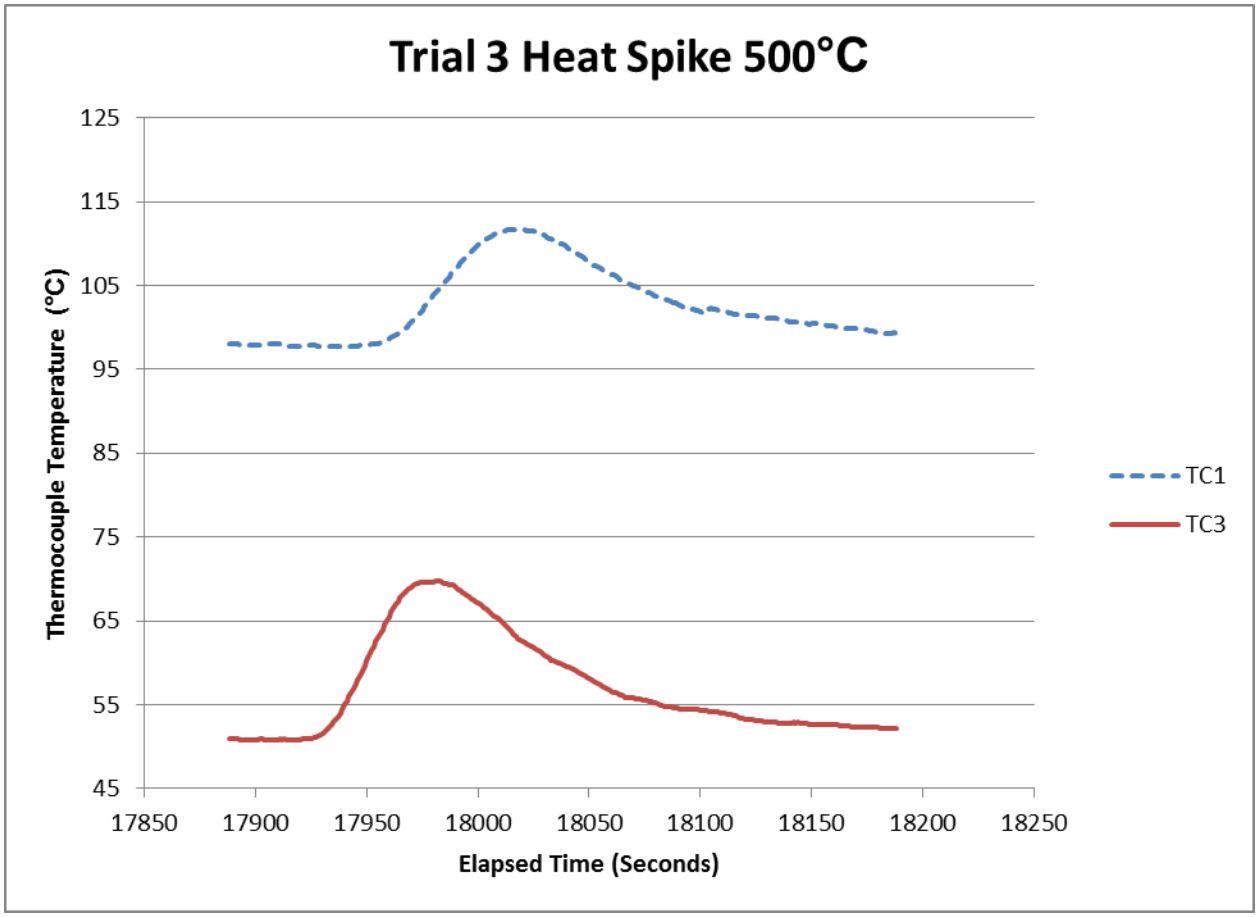
Trial 3 Heat Spike 500°C
Thermocouple Temperature (°C)
125
115
105
95
85
75
65
55
45
17850
17900
17950
18000
18050
18100
18150
18200
18250
Elapsed Time (Seconds)
TC1
TC3

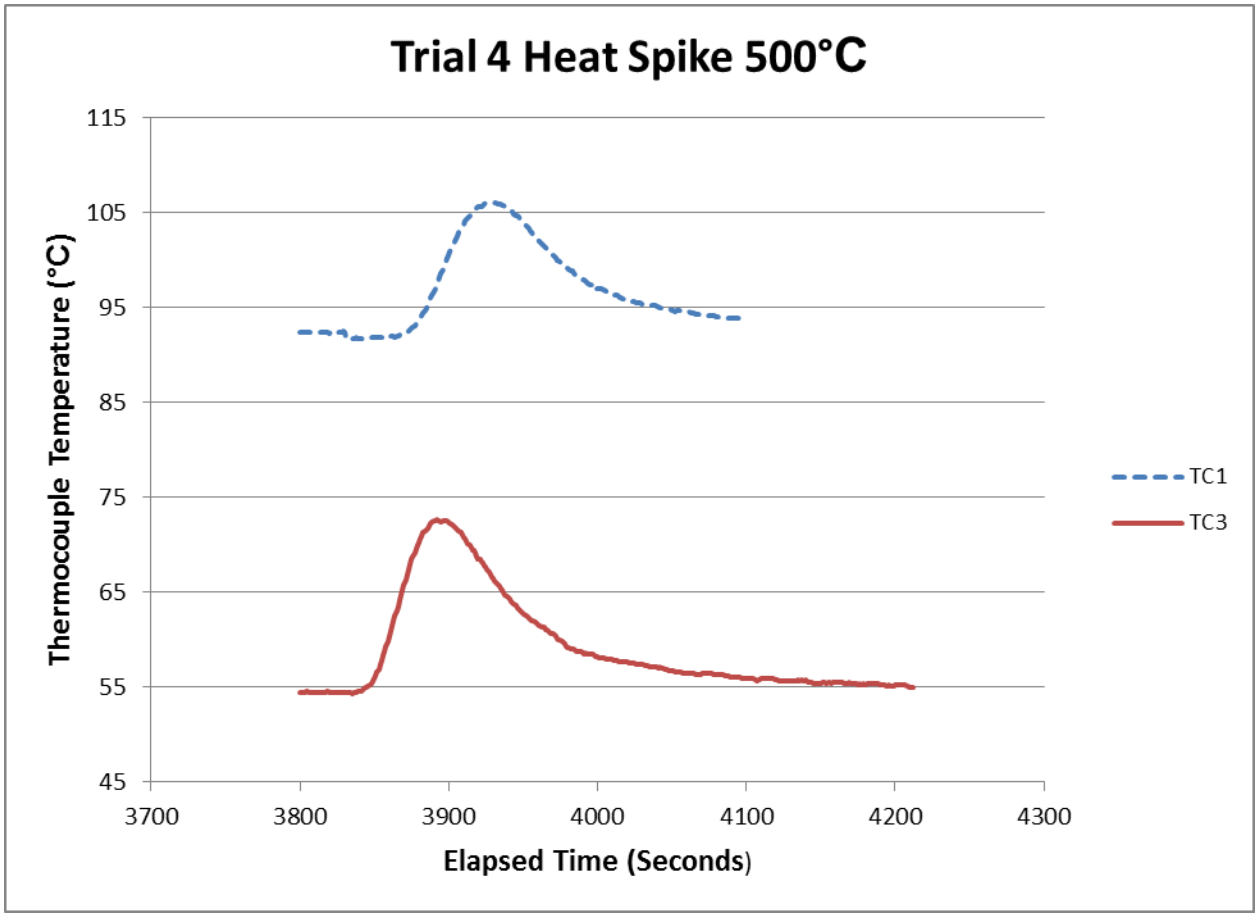
Trial 4 Heat Spike 500°C
Thermocouple Temperature (°C)
115
105
95
85
75
65
55
45
3700
3800
3900
4000
4100
4200
4300
Elapsed Time (Seconds)
TC1
TC3

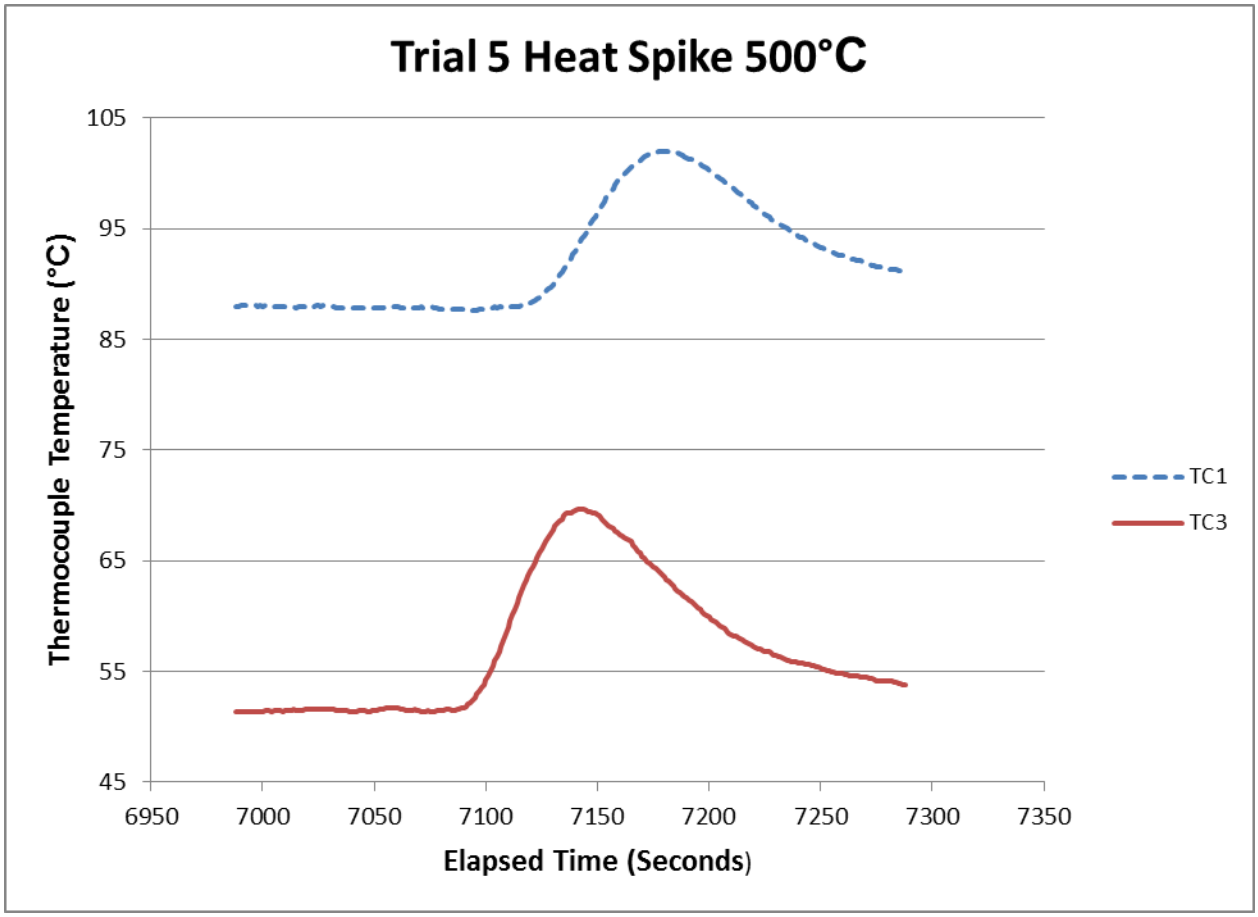
Trial 5 Heat Spike 500°C
Thermocouple Temperature (°C)
105
95
85
75
65
55
45
6950
7000
7050
7100
7150
7200
7250
7300
7350
Elapsed Time (Seconds)
TC1
TC3

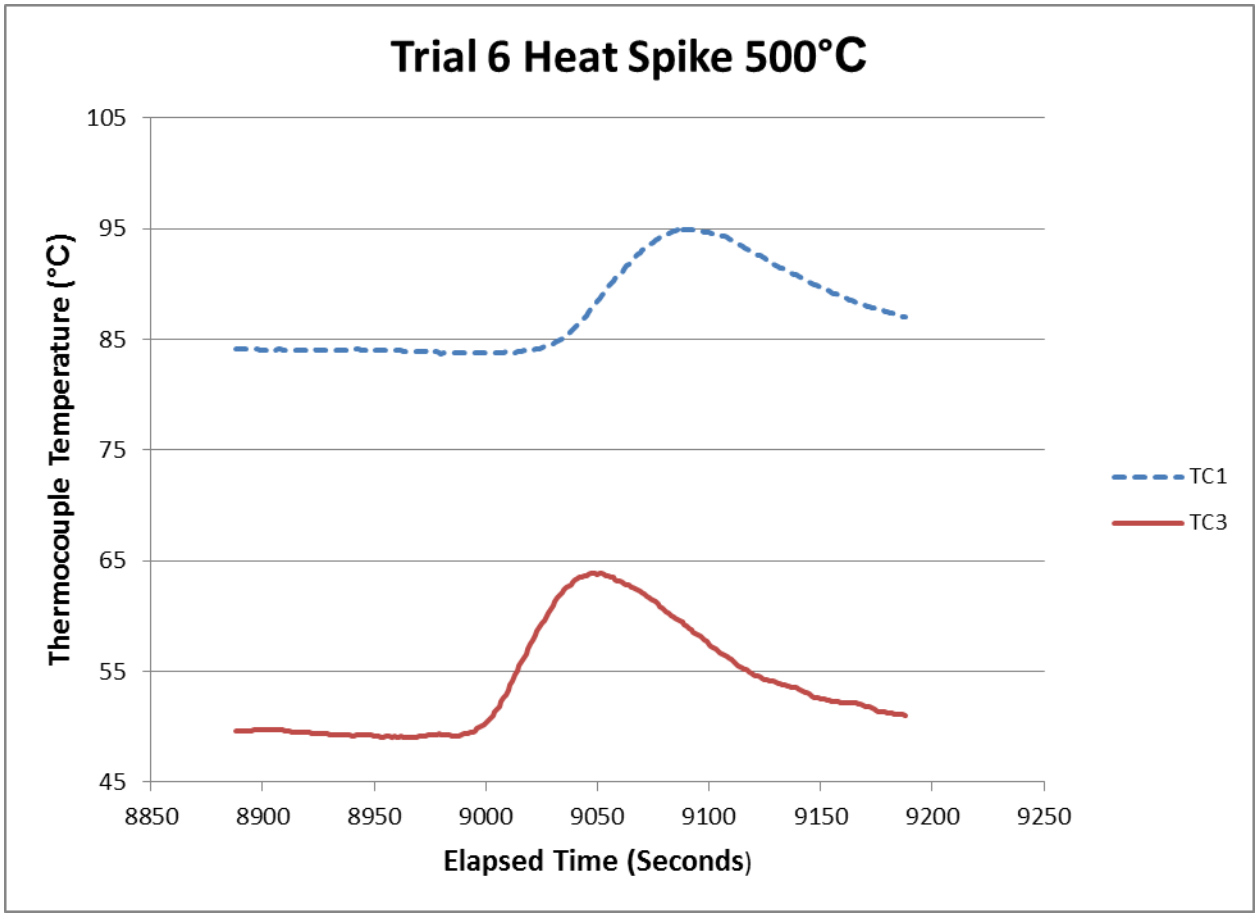
Trial 6 Heat Spike 500°C
Thermocouple Temperature (°C)
105
95
85
75
65
55
45
8850
8900
8950
9000
9050
9100
9150
9200
9250
Elapsed Time (Seconds)
TC1
TC3

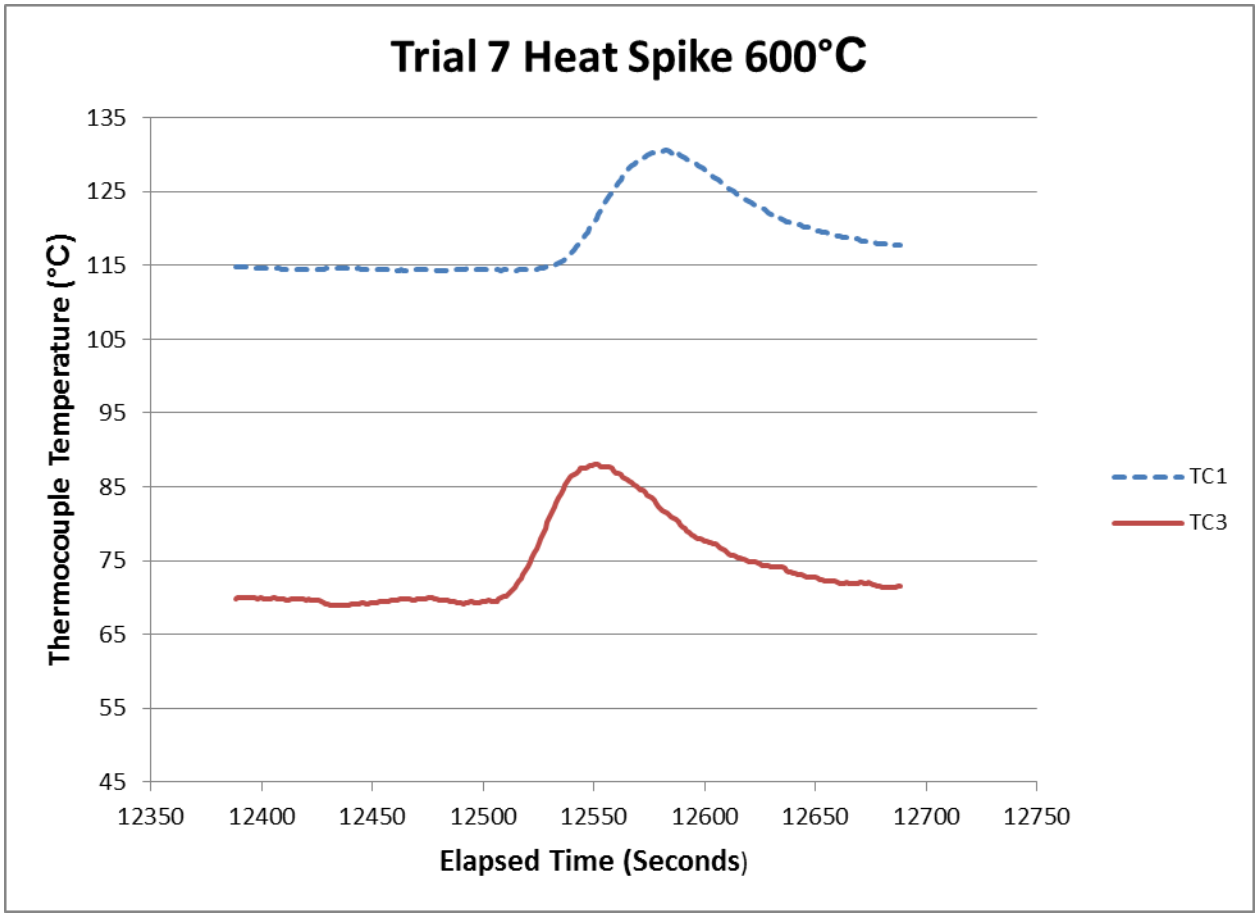
Trial 7 Heat Spike 600°C
Thermocouple Temperature (°C)
135
125
115
105
95
85
75
65
55
45
12350
12400
12450
12500
12550
12600
12650
12700
12750
Elapsed Time (Seconds)
TC1
TC3

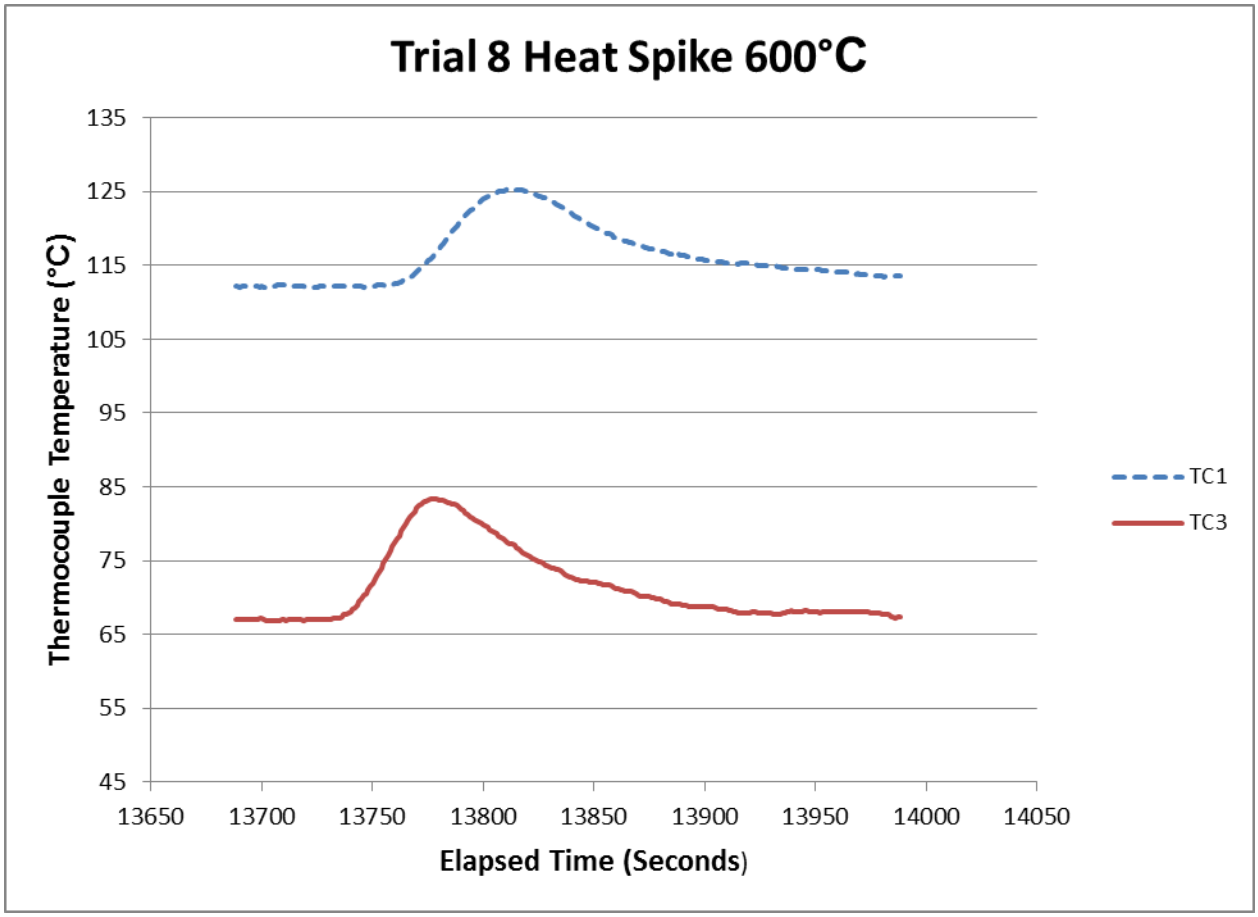
Trial 8 Heat Spike 600°C
Thermocouple Temperature (°C)
135
125
115
105
95
85
75
65
55
45
13650
13700
13750
13800
13850
13900
13950
14000
14050
Elapsed Time (Seconds)
TC1
TC3

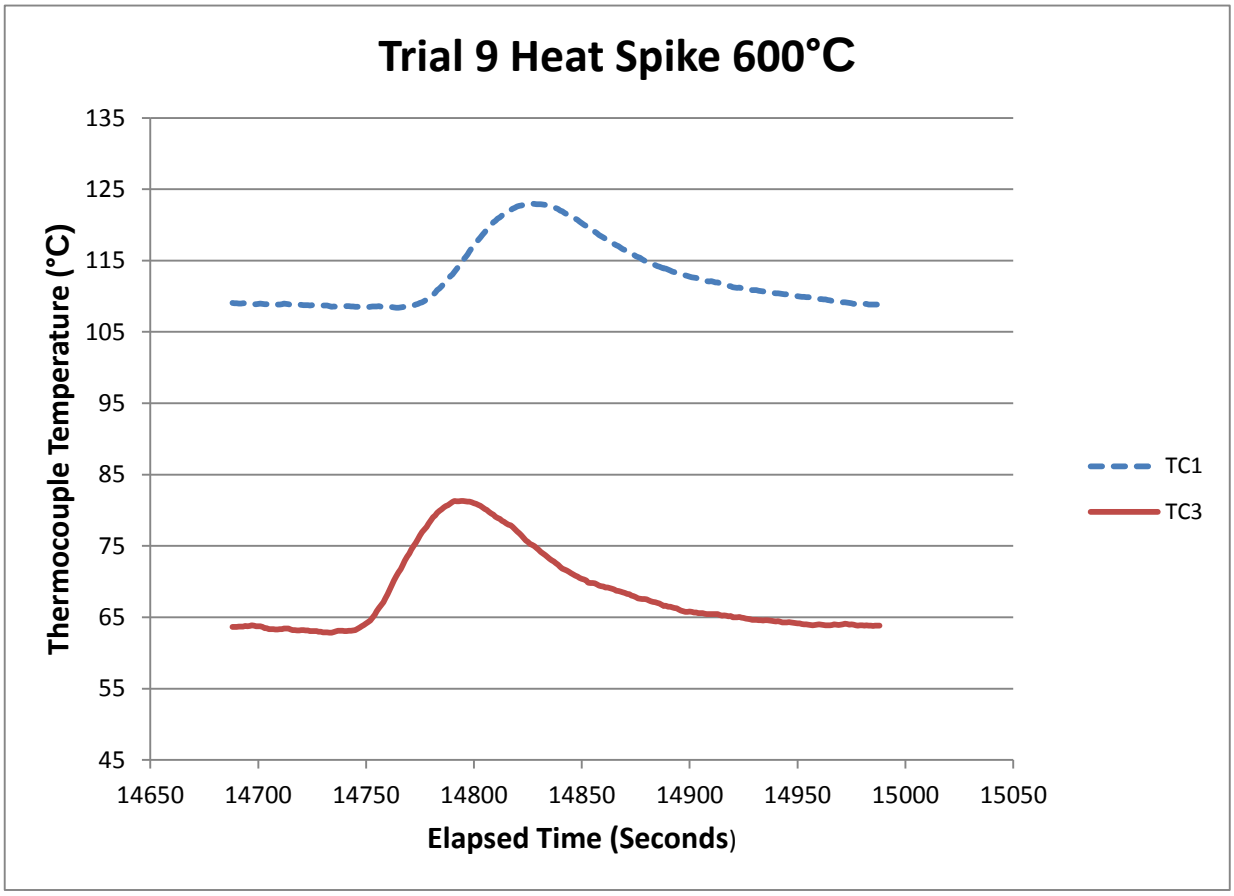
Trial 9 Heat Spike 600°C
Thermocouple Temperature (°C)
135
125
115
105
95
85
75
65
55
45
14650
14700
14750
14800
14850
14900
14950
15000
15050
Elapsed Time (Seconds)
TC1
TC3

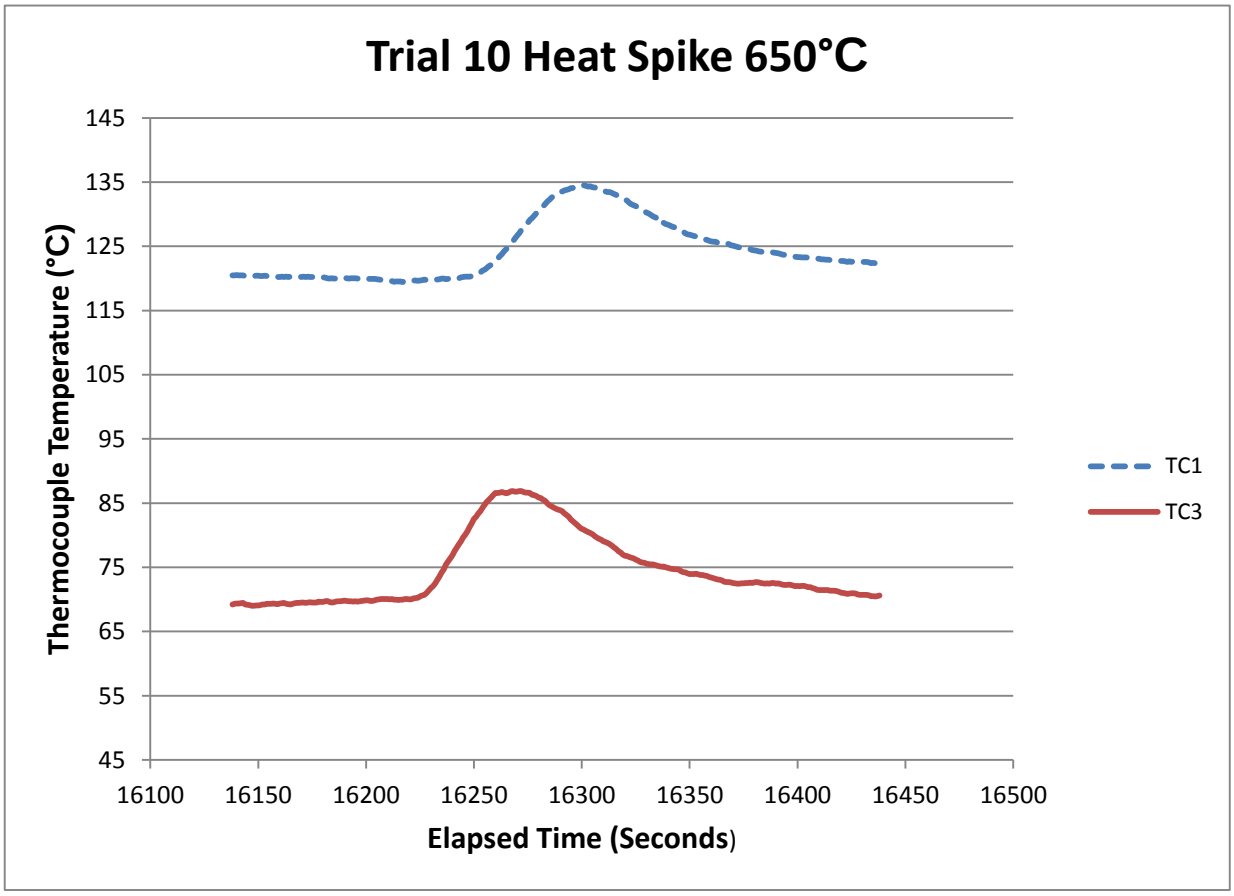
Trial 10 Heat Spike 650°C
Thermocouple Temperature (°C)
145
135
125
115
105
95
85
75
65
55
45
16100
16150
16200
16250
16300
16350
16400
16450
16500
Elapsed Time (Seconds)
TC1
TC3

Appendix B

NaK Flow Calculation:

$$A_{xs-furnace} = \pi \frac{\left(D_{furnace}\right)^2}{4} = 0.0029 m^2$$

$$A_{xs-tube} = \pi \frac{(D_{tube})^2}{4} = 9.284 \times 10^{-5} m^2$$

$$A_{xs-HX} = \pi \frac{(D_{HX})^2}{4} = 9.284 \times 10^{-5} m^2$$

$$\left(\frac{L}{D}\right)_{furnace} = 4.84$$

$$\left(\frac{L}{D}\right)_{tubing} = 142.5$$

$$\left(\frac{L}{D}\right)_{HX} = 14.02$$

$where\ D = inner\ diameter\ of\ tubing\ in\ meters$

$A_{xs} = cross - sectional\ area\ of\ tubing\ in\ m^2$

$and\ L = length\ of\ tubing\ in\ meters$

$$Re = \frac{\rho \times v \times D}{\mu} = \frac{808.3 \times 0.0031 \times 0.0108712}{5.69 \times 10^{-4}} = 47.874$$

$where\ v = linear\ velocity\ in\ m/s$

$\rho = average\ NaK\ density\ for\ the\ loop\ in\ kg/m^3$

$\mu = dynamic\ viscosity\ for\ furnace\ temperature\ in\ Pa * s$

$Re = Reynolds\ number$

Assumptions:

1.) Laminar Flow due to low Reynolds number
2.) No heat loss in tubing or furnace
3.) No flow losses in tube bends/elbows
4.) Steady State

Assuming steady state flow and neglecting local losses gives:

$$\Delta P_{buoyancy} = \Delta P_{viscous}$$

$where\ \Delta P_{buoyancy} = pressure\ changes\ from\ temperature\ density\ changes$

$\Delta P_{viscous} = pressure\ changes\ in\ the\ loop\ from\ viscousity\ changes$

$$\Delta P_{viscous} = \Delta P_{furnace} + \Delta P_{tube} + \Delta P_{HX}$$

$\Delta P_{furn} = change\ in\ NaK\ pressure\ in\ the\ furnace$

$\Delta P_{tube} = change\ in\ NaK\ pressure\ in\ the\ tube$

$\Delta P_{HX} = change\ in\ NaK\ pressure\ in\ the\ heater\ exchanger$

$$\Delta P_{furnace} = \left(\frac{1}{2}\rho v_{furn}^2\right) f_{furn} \left(\frac{L}{D}\right)_{furn}$$

$$v_{furn} = \frac{W_L}{A_{xs-furn} \times \rho}$$

$$f_{furn} = \frac{64}{Re} = \frac{64}{\frac{\rho \times v_{furn} \times D_{furn}}{\mu_{furn}}} = \frac{64}{\frac{W_L \times D_{furn}}{A_{xs-furn} \times \mu_{furn}}}$$

$where\ v_{furn} = linear\ velocity\ in\ the\ furnace\ in\ m/s$

$\rho = average\ NaK\ density\ for\ the\ loop\ in\ kg/m^3$

$Re_{furn} = Reynolds\ number$

$W_L = loop\ mass\ flow\ rate\ in\ kg/sec$

$\mu_{furn} = dynamic\ viscosity\ for\ furnace\ temperature\ in\ Pa * s$

Substituting terms into $\Delta P_{furnace}$ gives:

$$\Delta P_{furnace} = \frac{1}{2}(64)\frac{1}{\rho}\left(\frac{W_L}{A_{xs-furn}}\right)\left(\frac{\mu_{furn}}{D_{furn}}\right)\left(\frac{L}{D}\right)_{furn}$$

Treating ΔP_{tube} and ΔP_{HX} the same gives:

$$\Delta P_{tube} = \frac{1}{2}(64)\frac{1}{\rho}\left(\frac{W_L}{A_{xs-tube}}\right)\left(\frac{\mu_{tube}}{D_{tube}}\right)\left(\frac{L}{D}\right)_{tube}$$

$$\Delta P_{HX} = \frac{1}{2}(64)\frac{1}{\rho}\left(\frac{W_L}{A_{xs-HX}}\right)\left(\frac{\mu_{HX}}{D_{HX}}\right)\left(\frac{L}{D}\right)_{HX}$$

$$\Delta P_{viscous} = \frac{1}{2}(64)\frac{1}{\rho}W_L\left\{\left[\frac{\mu}{A_{xs} \times D} \times \frac{L}{D}\right]_{furn} + \left[\frac{\mu}{A_{xs} \times D} \times \frac{L}{D}\right]_{tube} + \left[\frac{\mu}{A_{xs} \times D} \times \frac{L}{D}\right]_{HX}\right\}$$

$$\Delta P_{buoyancy} = [-\rho(T_{hot}) + \rho(T_{cold})]g \times h$$

$where\ \rho(T_{hot}) = density\ of\ the\ NaK\ in\ the\ hot\ leg\ in\ kg/m^3$

$\rho(T_{cold}) = density\ of\ the\ NaK\ in\ the\ cold\ leg\ in\ kg/m^3$

$g = gravity\ acceleration\ in\ m/s^2$

$h = height\ between\ centers\ of\ the\ furnace\ and\ heat\ exhanger\ in\ meters$

Substitute values for $\Delta P_{buoyancy} = \Delta P_{loop}$:

$$[-\rho(T_{hot}) + \rho(T_{cold})]g \times h = \frac{1}{2}(64)\frac{1}{\rho}W_L\left\{\left[\frac{\mu}{A_{xs} \times D} \times \frac{L}{D}\right]_{furn} + \left[\frac{\mu}{A_{xs} \times D} \times \frac{L}{D}\right]_{tube} + \left[\frac{\mu}{A_{xs} \times D} \times \frac{L}{D}\right]_{HX}\right\}$$

Solve for W_L:

$$W_L = \frac{[-\rho(T_{hot}) + \rho(T_{cold})]g \times h}{\frac{1}{2}(64)\frac{1}{\rho}\left\{\left[\frac{\mu}{A_{xs} \times D} \times \frac{L}{D}\right]_{furn} + \left[\frac{\mu}{A_{xs} \times D} \times \frac{L}{D}\right]_{tube} + \left[\frac{\mu}{A_{xs} \times D} \times \frac{L}{D}\right]_{HX}\right\}}$$

Input numerical values:

$\rho(T_{hot}) = 833.5\frac{kg}{m^3}$ $\rho(T_{cold}) = 883.5\frac{kg}{m^3}$ $g = 9.81\frac{m}{s^2}$ $h = 0.0254\ m$

$\mu_{furn} = 1.42 \times 10^{-4}\ Pa \times s;$ $A_{xs-furn} = 0.0029\ m^2;$

$\left(\frac{L}{D}\right)_{furn} = 4.84;$ $D_{furn} = 0.060325\ m$

$\mu_{tube} = 3.22 \times 10^{-4}\ Pa \times s;$ $A_{xs-tube} = 9.284 \times 10^{-5}\ m^2;$

$\left(\frac{L}{D}\right)_{tube} = 142.52;$ $D_{tube} = 0.01087\ m$

$\mu_{HX} = 5.69 \times 10^{-4}\ Pa \times s;$ $A_{xs-HX} = 9.284 \times 10^{-5}\ m^2;$

$\left(\frac{L}{D}\right)_{HX} = 14.02;$ $D_{HX} = 0.01087\ m$

$W_L = 0.005896\ kg/s$

$v_{tube} = .0786\frac{m}{sec} = 78.6\ mm/s$

Vita

David Joseph Rowekamp was born in Cincinnati, Ohio in the United States of America on June 13th, 1986. He achieved his basic elementary and high school education in the same city. He received his bachelor's degree in Biomedical engineering from the University of Cincinnati in the spring of 2010. In August 2010, he accepted admission for a Master's degree program in Nuclear Engineering from the University of Tennessee, Knoxville, working as a Graduate Assistant for Dr. Martin Grossbeck. This Master's degree is to be awarded to him by August 2013. David is planning to work as a Nuclear Engineer, where he will gain the experience necessary to match engineering knowledge.